Cell Reports

Article

The nucleoporin Nup153 is the anchor for Kif1a during basal nuclear migration in brain progenitor cells

Graphical abstract

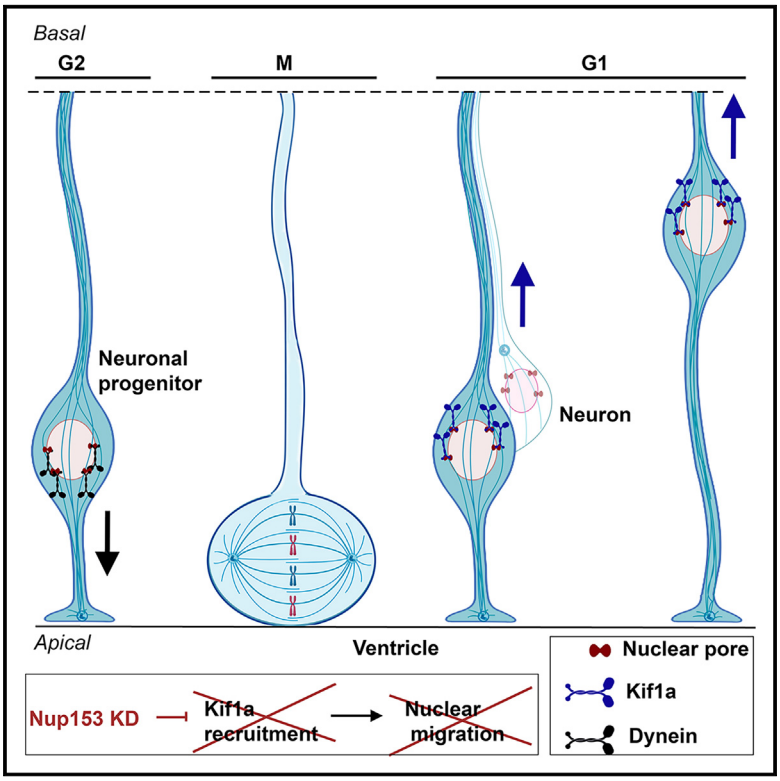

Authors

Aditi Falnikar, Sebastian Quintremil, Hung-Jun Zhao, Haw-Yuan Cheng, Paige Helmer, Jin-Wu Tsai, Richard B. Vallee

Correspondence

aditi.falnikar@gmail.com (A.F.), rv2025@cumc.columbia.edu (R.B.V.)

In brief

Falnikar et al. report that the nucleoporin Nup153, a binding partner of microtubule motor protein Kif1a, originally identified in a proteomic study, recruits Kif1a to the radial glial progenitor (RGP) cell nuclear envelope to drive basal nuclear migration and also causes an increase in G1-phase RGP cells.

Highlights

- Nup153 RNAi inhibits basal INM in RGP cells
- Kif1a decorates nuclear envelope (NE) in RGP cells
- Kif1a NE localization is lost upon Nup153 RNAi

Falnikar et al., 2024, Cell Reports *43*, 115008
December 24, 2024
https://doi.org/10.1016/j.celrep.2024.115008

CellPress

Cell Reports

CellPress
OPEN ACCESS

Article

The nucleoporin Nup153 is the anchor for Kif1a during basal nuclear migration in brain progenitor cells

Aditi Falnikar,[1,3,*] Sebastian Quintremil,[1] Hung-Jun Zhao,[2] Haw-Yuan Cheng,[2] Paige Helmer,[1] Jin-Wu Tsai,[2] and Richard B. Vallee[1,*]

[1]Department of Pathology and Cell Biology, Columbia University Medical Center, New York, NY 10032, USA
[2]Institute of Brain Science, College of Medicine, National Yang Ming Chiao Tung University, Taipei 112, Taiwan
[3]Lead contact
*Correspondence: aditi.falnikar@gmail.com (A.F.), rv2025@cumc.columbia.edu (R.B.V.)
https://doi.org/10.1016/j.celrep.2024.115008

SUMMARY

Radial glial progenitors (RGPs) are highly elongated epithelial cells that give rise to most stem cells, neurons, and glia in the vertebrate cerebral cortex. During development, the RGP nuclei exhibit a striking pattern of cell-cycle-dependent oscillatory movements known as interkinetic nuclear migration (INM), which we previously found to be mediated during G1 by the kinesin Kif1a and during G2 by cytoplasmic dynein, recruited to the nuclear envelope by the nucleoporins RanBP2 and Nup133. We now identify Nup153 as a nucleoporin anchor for Kif1a, responsible for G1-specific basal nuclear migration, providing a complete model for the mechanisms underlying this basic but mysterious behavior, with broad implications for understanding brain development.

INTRODUCTION

Radial glial progenitor (RGP) cells give rise to the majority of stem cells, neurons, and glia during development of the vertebrate neocortex.[1,2] RGPs are highly elongated epithelial cells with processes that span the wall of the neural tube and the developing cortex from its ventricular to pial surface. RGPs are highly proliferative[3] and also serve as scaffolds for the migration of postmitotic neurons,[4] thereby playing uniquely important roles in brain development.

RGP nuclei undergo a series of cell-cycle-dependent oscillatory movements known as interkinetic nuclear migration (INM).[5–10] Mitosis begins when the G2 nucleus reaches the apical end of the cell at the ventricular surface (VS) of the brain. The nucleus then migrates basally during G1, completes S phase away from the ventricle,[11] and returns to the VS during G2 for the next mitotic division. INM may be involved in cell fate determination[12] or maximizing the number of dividing cell bodies accommodated at the VS.[8]

We have reported roles for cytoplasmic dynein and Kif1a in INM and postmitotic neuronal migration using fixed and live imaging of embryonic rat brain.[6,7,9,11] The centrosomes remained at the VS during INM, with microtubules (MTs) within the apical processes, oriented uniformly with their minus ends toward the pial brain surface. Consistent with this arrangement, RNAi for the MT plus-end-directed kinesin, Kif1a, inhibited basal nuclear migration, whereas RNAi for cytoplasmic dynein or its regulator LIS1 inhibited apical migration.

Although centrosomes associate with nuclei during migration in many cell types, the centrosome-independent nuclear migration we observed in RGPs[7,13] suggested that the motor proteins in this case might act locally at the nuclear surface. In the case of rat RGPs, we found sequential G2-specific mechanisms responsible for dynein nuclear pore recruitment, involving, respectively, RanBP2-BicD2-dynein and Nup133-CENP-F-dynein interactions.[6,14–16]

In contrast to dynein recruitment to the RGP nuclear envelope (NE), nothing is known about an equivalent mechanism for Kif1a. Kif1a has well-established roles in higher eukaryotic transport of synaptic vesicle precursors[17–19] and other vesicular cargo.[20–24] Human KIF1A mutations have also been implicated in severe, progressive neurological disease.[25,26]

The current study was undertaken to define the mechanisms responsible for Kif1a-mediated basal nuclear migration and determine the region within Kif1a that binds the nucleus. To this end, we took advantage of a recently published Kif1a interactome.[27] Among the hits is a nucleoporin—Nup153.

We report here that Nup153 RNAi inhibits basal INM in RGP cells. Endogenous Kif1a colocalizes with the C-terminal region of Nup153 in HeLa cells. Expression of a Kif1a fragment that binds to Nup153 exhibits clear NE decoration in HeLa cells, as well as RGP cells and postmitotic neurons, and is lost upon Nupe153 RNAi, suggesting a general mechanism for nuclear transport.

RESULTS

Identification of NE-associated Kif1a interactors

To identify potential NE-associated Kif1a interactors, we took advantage of data obtained in a recent Kif1a interactome

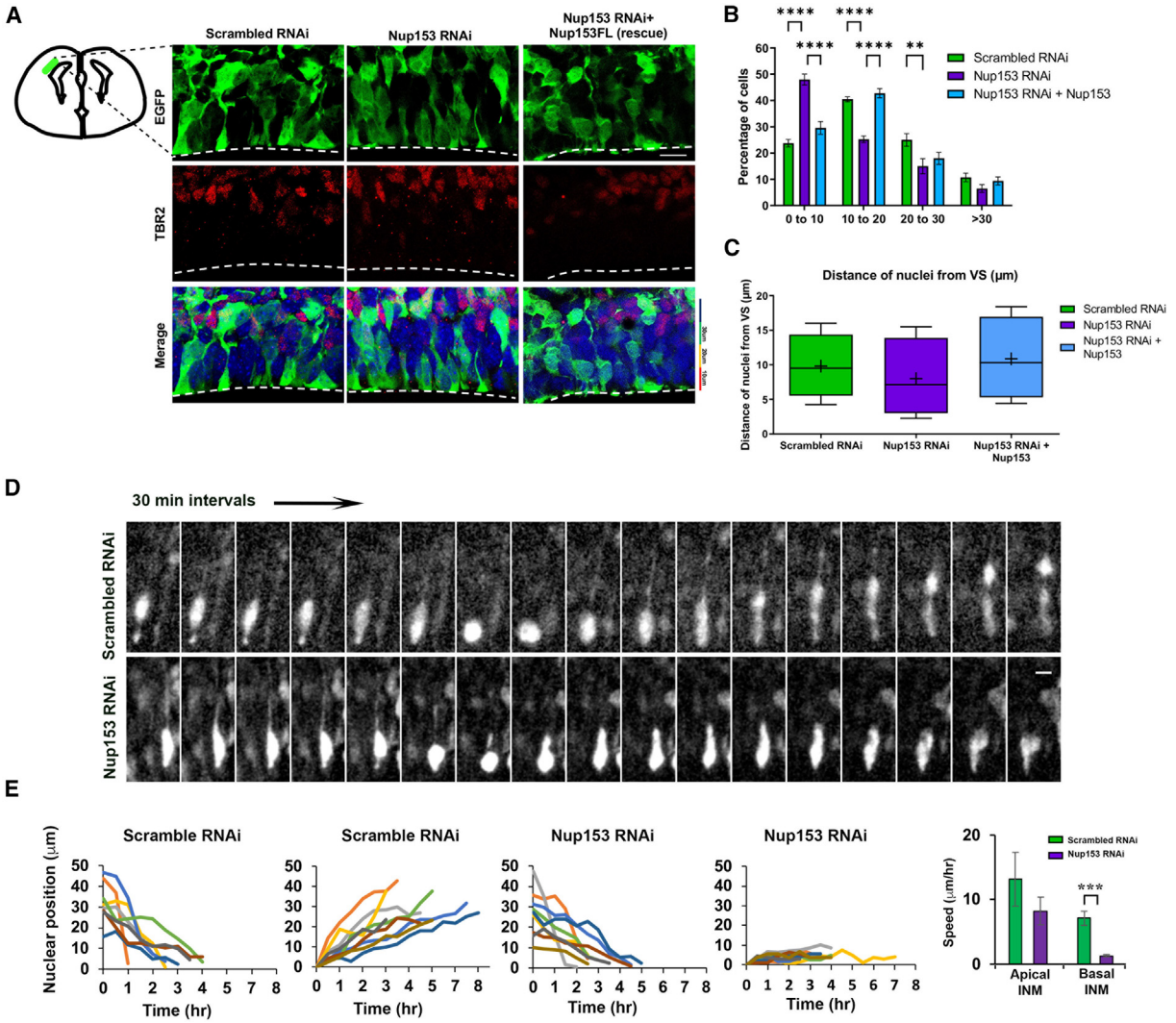

Figure 1. Nup153 is required for basally directed nuclear movement in RGPs

E16 embryonic brains were *in utero* electroporated with scrambled shRNA, Nup153 shRNAs, or Nup153 shRNA and RNAi-resistant human full-length HA-Nup153 constructs and subsequently imaged live or fixed 3 days post-injection at E19.

(A) Fixed images of the VZ from electroporated brains stained for EGFP and Tbr2. Dashed line represents the VS. KIF1A RNAi caused clear accumulation of RGP somata near the VS. The presence of the radial glial basal process indicates retention of overall cell morphology. Tbr2 staining was used to exclude intermediate precursors.

(B and C) Quantification of distance between the RGP nuclei and the VS across conditions. Control nuclei were distributed at a range of distances from the ventricular surface. Nuclei of Nup153 shRNA-expressing cells accumulated relatively closer to the VS. Clear rescue of this phenotype was observed with co-expression of human full-length HA-Nup153. (scramble shRNA, $n = 4$; Nup153 shRNA, $n = 4$; Nup153 shRNA + human full-length-Nup153, $n = 5$; $^{**}p < 0.01$, $^{***}p < 0.001$, and $^{****}p < 0.0001$; error bars = SEM).

(D) Time-lapse images for scrambled shRNA or Nup153 shRNA in RGPs (Videos S1 and S2). Images are shown at 30-min intervals. Scale bar: 10 μm.

(E) Quantification of movement of RGP nuclei. Tracings of movements of individual nuclei in scrambled shRNA- or Nup153 shRNA-expressing RGP cells show that there was no apparent effect of Nup153 RNAi in the apical direction. In contrast, marked effects are observed in the basal direction for all RGP nuclei. The speed of apical INM was higher than that of basal INM in each condition.

study.[27] We found five candidate proteins for NE binding. Four are nucleoporins, whereas the remaining one was an mRNA export factor, Rae1, which we did not consider for further analysis. Of the four nucleoporins, we focused on the only one with a high SAINT score (0.98), Nup153. Of the remaining three nucleoporins (Nup88, Nup160, Nup214) with low SAINT scores, Nup160 was randomly chosen as a negative control.

Role of Nup153 in INM in RGP cells

To test the role of a potential Kif1a recruitment factor specifically during INM, we expressed short hairpin RNAs (shRNAs) for Nup153 (Figure S1) and Nup160, as well as a Nup153 scrambled shRNA, using *in utero* electroporation in embryonic day (E)16 rat brain. We imaged RGP cells in fixed brain slices 3 days after *in utero* electroporation. Nup153 knockdown (KD) caused

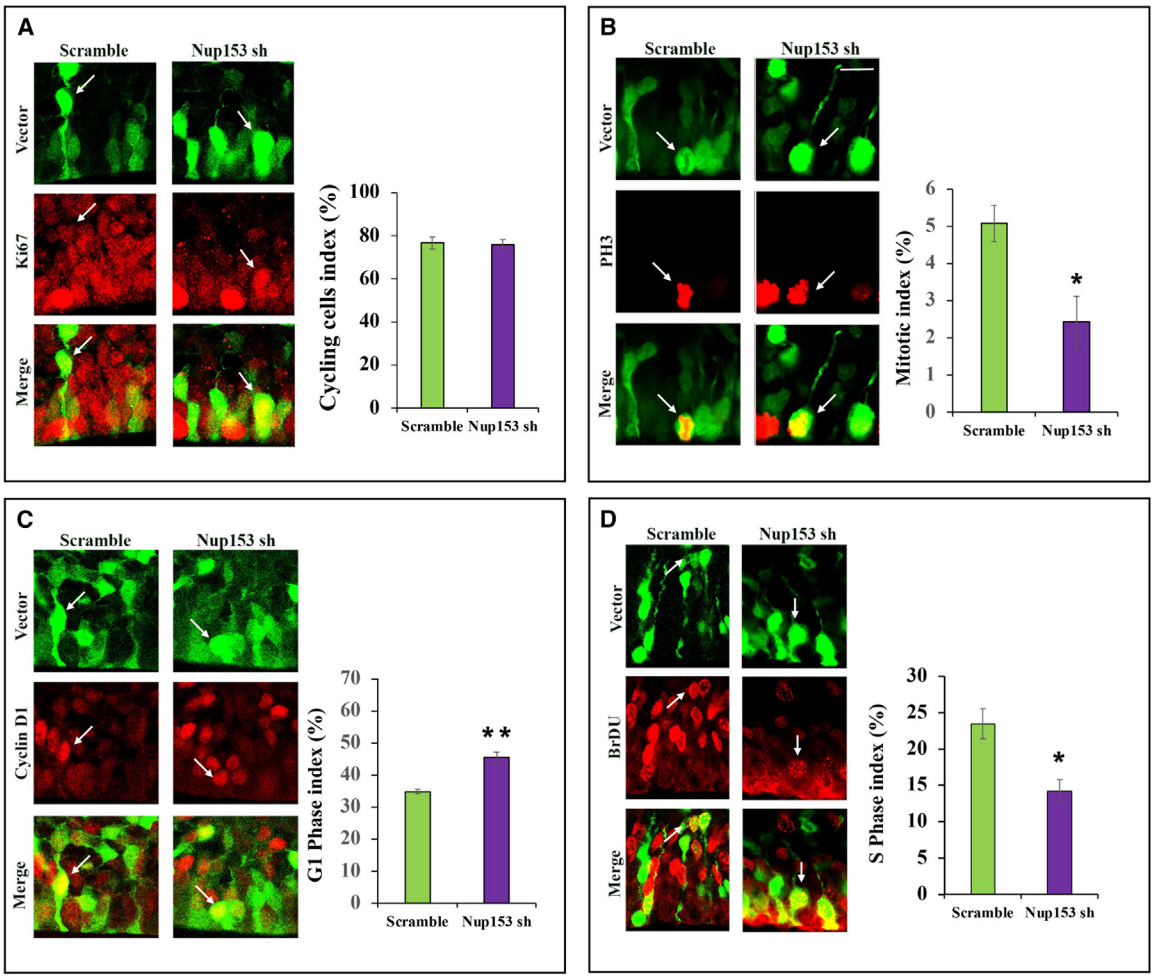

Figure 2. Nup153 RNAi in RGP cells leads to an increase in G1-phase cells

(A–D) E16 embryonic brains were *in utero* electroporated with either scrambled shRNA or shRNA for Nup153. Brains were then fixed at E19 and stained with cell cycle markers as follows: Ki67 (cycling cells), cyclin D1 (G1 phase), and phospho-histone H3 (PH3) (late G2/M phases). We also investigated the effect of Nup153 RNAi on S phase by BrdU pulse labeling. Comparable percentages of control and Nup153 knockdown RGP cells expressed Ki67, suggesting that Nup153 has no gross effect on the fraction of cycling cells, although a subpopulation in each case escaped the cell cycle. There was a significant increase in the percentage of RGP cells positive for cyclin D1 and a corresponding decrease in the percentage of RGP cells positive for PH3 as well as BrdU (scramble shRNA, $n = 3$; Nup153 shRNA, $n = 3$; $^{**}p < 0.01$ and $^{***}p < 0.001$; error bars = SEM). Scale bar: 15 μm.

significant accumulation of RGP somata within 10 μm of the VS, though cell morphology was unaffected, and basal processes still extended to the pial surface of the brain. Neither Nup160 nor scrambled Nup153 shRNAs affected the distribution of RGPs somata (Figures 1A–1C, S2, and S3).

As a further test for a role for Nup153 in nuclear migration, we co-expressed RNAi-insensitive human hemagglutinin (HA)-tagged Nup153 with a Nup153 shRNA. Nup153 expression alone produced no detectable phenotype. However, clear rescue of nuclear distribution by HA-HuNup153 was observed (Figures 1A–1C).

To test the role of Nup153 more directly, we performed live imaging of RGPs. Consistent with fixed tissue analysis, live-cell imaging revealed specific inhibition of basal INM in RGPs upon Nup153 RNAi, with nuclei remaining within ~15 μm of the VS throughout the recording period (Figures 1D and 1E; Videos S1, S2, S3, and S4). Some short departures from the VS could be seen, possibly due to residual Nup153 expression or passive nuclear displacement.

Our results, together, indicate that KD of Nup153 blocks the basal INM, thus phenocopying Kif1a RNAi.

Role of Nup153 in RGP cell cycle progression

We previously found that Kif1a RNAi does not affect cell cycle progression,[11] suggesting that cell cycle progresses normally despite inhibition of basal INM. To test for the effect of Nup153 RNAi, we stained Nup153 shRNA-expressing brain sections with cell cycle markers. While Nup153 RNAi had no gross effect on the fraction of Ki67-positive cycling cells, it caused a significant increase in cyclin D1-positive G1-phase cells with a concomitant decrease in cells in S phase as well as those expressing phospho-histone H3, a marker for G2/M phase (Figures 2A–2D and S4). In

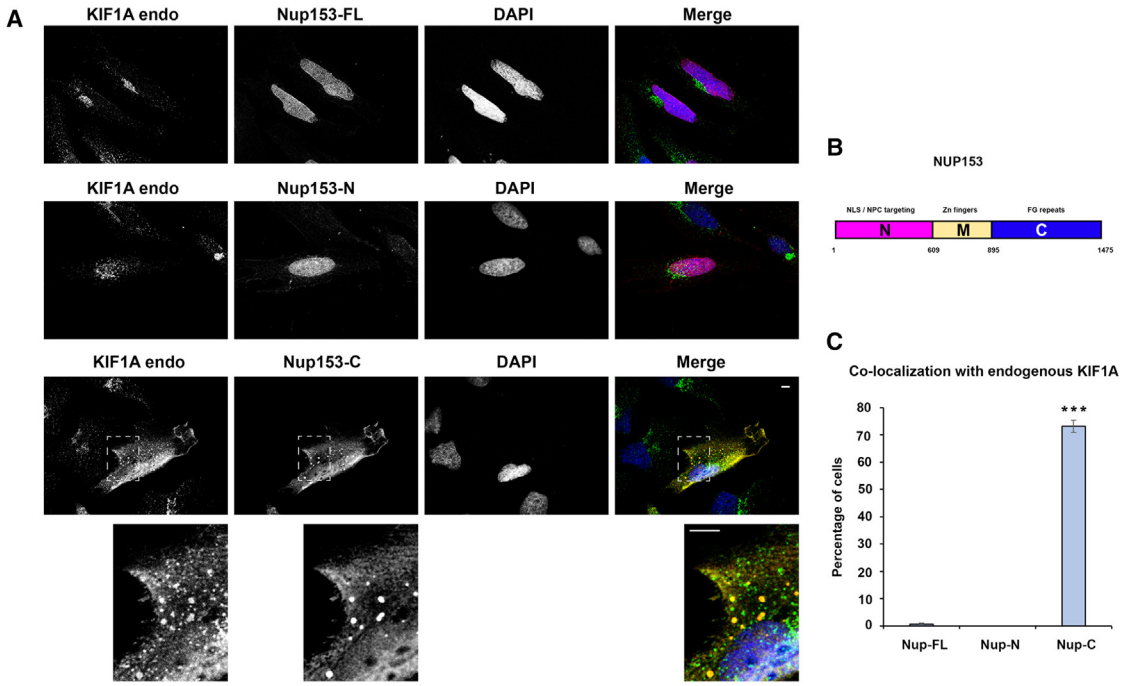

Figure 3. The C-terminal domain of Nup153 colocalizes with the endogenous Kif1a

(A) HeLa cells expressing the full-length N-terminal, or C-terminal domain of Nup153 with mCherry tag that is fused at its N terminus are stained for endogenous Kif1a. Areas in the white dotted boxes are enlarged on the bottom. Endogenous KIF1 shows clear colocalization with the Nup153-C fragment. Scale bars: 5 μm.

(B) Schematic representation of Nup153 molecule.

(C) Quantification of colocalization between Kif1a tail fragment and Nup153 fragments (**$p < 0.01$ and ***$p < 0.001$; error bars = SEM).

these experiments, the effect of Nup153 RNAi on S phase was analyzed by either bromodeoxyuridine (BrdU) or 5-ethyl-2′-deoxyuridine (EdU) pulse labeling.[11]

These results, together, indicate that Nup153 regulates cell cycle progression in RGP cells. This is consistent with previous reports indicating a role for Nup153 in cell cycle regulation.[28–30] In particular, Nup153 RNAi significantly increased the percentage of G1-phase RGP cells. This phenotype has been previously reported in HeLa cells.[31]

Mechanistic insight from the Nup153 functional domains

To understand the relative role of Nup153's functional domains in anchoring Kif1a to the RGP nucleus, we next expressed previously characterized cDNA's encoding individual Nup153 domains[32] in E16 brains. The N-terminal portion of Nup153 (Nup153-N) contains the NE- and nuclear pore complex (NPC)-targeting sequences[33,34] and localizes to the NE in HeLa cells. The Nup153 C-terminal domain (Nup153-C) is flexible and extends to the cytoplasmic surface of the NPC.[35–37] Expression of Nup153-C or Nup153-full-length constructs in E16 brains had no detectable effect on RGP nuclear distribution. Interestingly, expression of Nup153-N resulted in a pronounced impairment of basal INM, similar to Nup153 KD (Figure S5). Together, these results suggest that the Nup153-N competes with endogenous Nup153 for NPC incorporation but is, by itself, insufficient to anchor Kif1a to the nucleus, presumably because the Kif1a-binding site lies elsewhere within the Nup153 molecule. These results confirm the role of Nup153 in anchoring Kif1a to the nucleus for basal nuclear migration.

Colocalization of Nup153 with Kif1a in nonneural cells

To further understand the role of Nup153 in NE Kif1a recruitment, we tested for co-distribution of Nup153 with endogenous as well as recombinant Kif1a in nonneuronal cells. Interestingly, the Nup153-C showed a striking pattern of colocalization with the endogenous Kif1a puncta (Figure 3).

To test whether Nup153 also associates with the tail region of Kif1a (amino acids 657–1105) that was originally used to pull down Nup153 from adult rat brain lysate, we monitored the potential colocalization of EGFP-tagged Nup153 and the mCherry-tagged Kif1a tail domain. When expressed by itself, the Kif1a tail domain showed a clear NE decoration in a majority of HeLa cells, consistent with its interaction with Nup153 (Figure 4). When expressed with Nup153, we again observed extensive diffuse as well as punctate colocalization of the Nup153-C with the Kif1a tail region (Figure 5).

Behavior of Kif1a tail region in RGP cells

Multiple proteins, including Nup153, were found to be associated with the KIF1A tail region in an earlier study.[27] The effect of Nup153 KD on basal INM supports our original proposal for Kif1a-mediated forces generated at the NE. To test whether

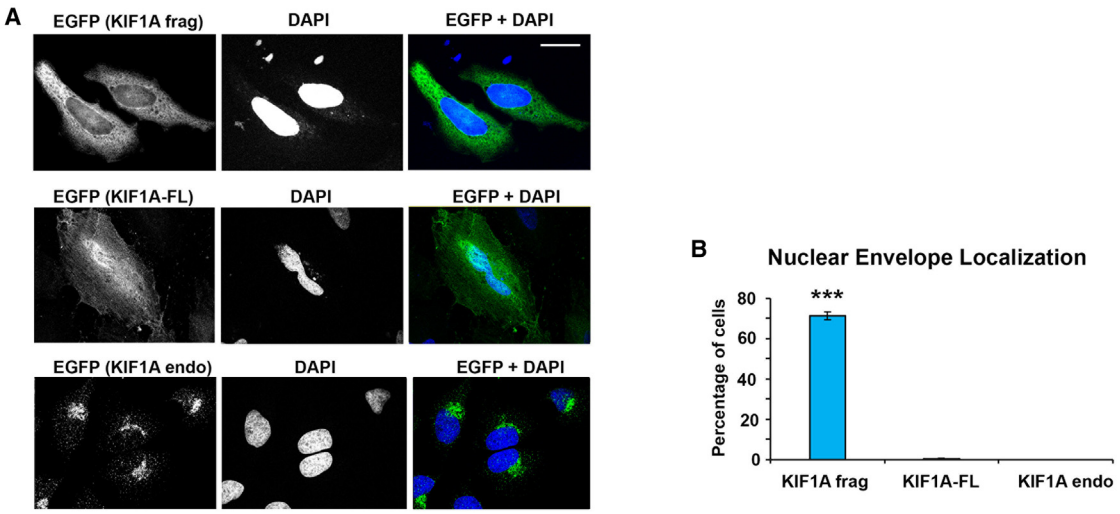

Figure 4. KIF1A tail fragment decorates NE in HeLa cells

(A) HeLa cells expressing KIF1A tail fragment with EGFP tag that is fused at its N terminus, fixed, and stained for EGFP. EGFP staining shows clear nuclear envelope (NE) decoration in a subset of cells, whereas NE decoration was not observed in HeLa cells expressing either full-length KIF1A or the ones stained with the anti-KIF1A antibody to detect endogenous KIF1A. Scale bar: 20 μm.

(B) Quantification of the fixed images of the HeLa cells expressing either KIF1A tail fragment or full length KIF1A and stained for EGFP to detect expression at the NE. Also included is the third condition, where HeLa cells were stained with anti-KIF1A antibody to detect the endogenous Kif1a expression at the NE. Only the HeLa cells expressing the KIF1A tail fragment showed NE localization. Each experiment was reproduced three independent times (over 50 cells per condition and per experiment were counted; $^{**}p < 0.01$ and $^{***}p < 0.001$; error bars = SEM).

the Kif1a tail region affects basal INM, we electroporated a cDNA encoding EGFP- as well as HA-tagged Kif1a tail region into E16 rat brain. As in HeLa cells, we observed clear NE decoration in most of the transfected RGP cells as well as in postmitotic neurons (Figures 6A and 6C). Expression of this domain also inhibited basal INM (Figures 6D and 6E), suggesting that the free Kif1a tail domain might compete with endogenous Kif1a for a common binding site at the NE. Our results, together, are consistent with the role of Nup153 in anchoring Kif1a, via its C-terminal domain, to the NE to drive basal nuclear migration.

Role of Nup153 in postmitotic neuronal migration

Previous work from our lab and others suggested that Kif1a participates in postmitotic neuronal migration as well.[11,38] Little is known about the mechanisms responsible for this behavior. To test whether this behavior shares mechanistic features with INM, we performed Nup153 RNAi and looked at the behavior of postmitotic neurons in fixed tissue. We found that brains subjected to Nup153 RNAi exhibited an almost complete absence of transfected cells within the IZ and cortical plate (CP) regions, unlike the control brains, consistent with a role for Nup153 in the recruitment of Kif1a to the NE to regulate neuronal migration (Figures S6 and S7). Most of the Nup153 shRNA-expressing cells were located in the sub-ventricular zone (SVZ) and exhibited a multipolar morphology, suggesting a defect in the multipolar-to-bipolar neuronal transition. This effect was similar to that observed for Kif1a KD. However, in Kif1a KD brains, neighboring non-transfected cells were also arrested in the SVZ in a multipolar state. Transfected cells and the neighboring cells also expressed Tbr1—a marker normally expressed only by the postmitotic projection neurons.[39,40] This non-cell-autonomous effect of Kif1a KD was not phenocopied by Nup153 KD, evidenced by the unaltered Tbr1 band in the Nup153 shRNA-expressing brains (Figure S6A).

Role of Nup153 in Kif1a NE recruitment

The Kif1a tail region was originally used to pull down Nup153 from adult rat brain lysate. This region localizes to the NE in non-neuronal cells, RGP cells, and postmitotic neurons, suggesting an important role for Nup153 in anchoring Kif1a to the NE. To test this directly, we used a commercially available Nup153 small interfering RNA (siRNA). Transfection of HeLa cells with this reagent reduced Nup153 expression as judged by immunostaining. Kif1a tail region expression in Nup153-depleted cells resulted in a dramatic loss of Kif1a NE localization (Figure 7). Additionally, Nup153 RNAi or Nup153-N expression resulted in loss of Kif1a NE localization in RGP cells as well (Figure S8). Together, these results indicate that Nup153 is necessary for Kif1a NE localization.

DISCUSSION

We previously found that INM is driven by kinesin- and dynein-mediated nuclear transport along uniformly oriented MTs.[7] During INM, the centrosome remains at the VS as the nucleus oscillates basally and apically. This centrosome-independent nuclear migration suggested that motor proteins may act from the nuclear surface, a relatively unusual mechanism in vertebrates. We now provide evidence that the kinesin Kif1a is present at the nuclear surface, and RNAi for a gene responsible for Kif1a nuclear recruitment inhibits INM.

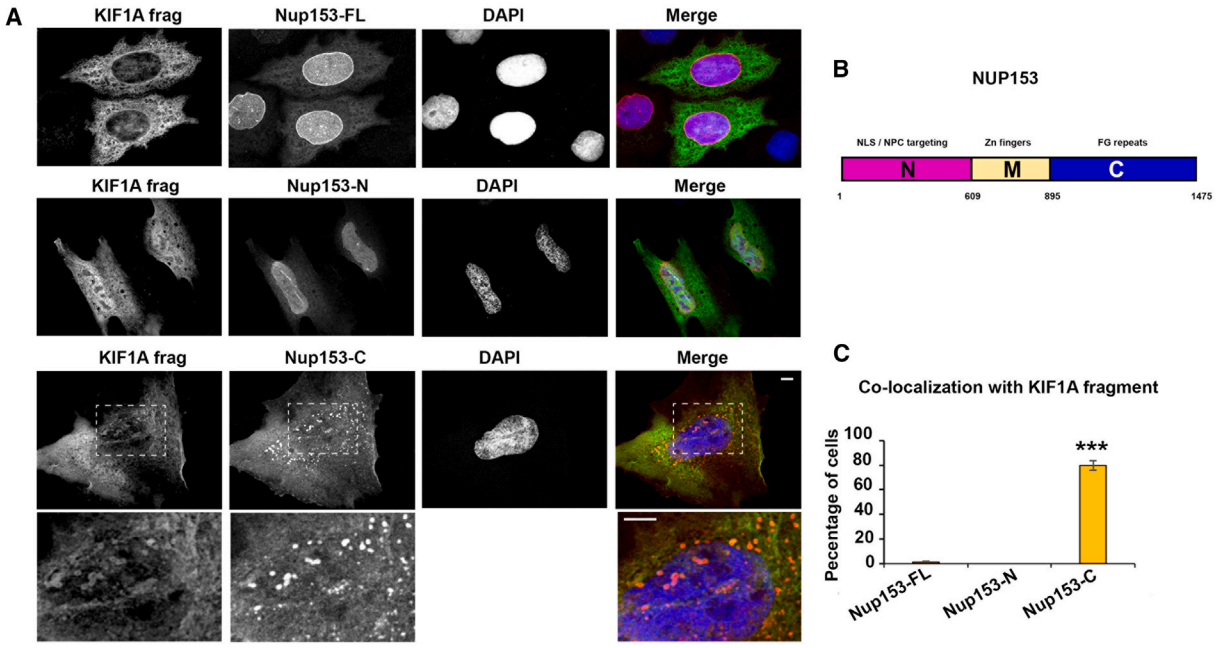

Figure 5. The C-terminal domain of Nup153 colocalizes with the recombinant Kif1a

(A) HeLa cells co-expressing KIF1A tail fragment with EGFP tag that is fused at its N terminus and full-length or N-terminal or C-terminal domains of Nup153 with mCherry tag that is fused at their N termini. Areas in the white dotted boxes are enlarged on the bottom. Endogenous KIF1a shows clear colocalization with the Nup153-C fragment. Scale bars: 5 μm.

(B) Schematic representation of Nup153 molecule.

(C) Quantification of colocalization between Kif1a tail fragment and Nup153 fragments (**$p < 0.01$ and ***$p < 0.001$; error bars = SEM).

Functional analysis in brain

We employed RNAi to investigate Nup153's role in INM, revealing strong inhibition of basal, but not apical, INM in RGP cells in embryonic rat brain, as judged by live imaging and fixed tissue analysis. A previous study demonstrated that Nup153 depletion does not impair general nucleocytoplasmic transport in HeLa cells,[29] suggesting an alternative mechanism for INM inhibition in RGPs. Our data confirm Kif1a's role in basal INM, supporting a role for the specific Kif1a sub-fraction associated with the NE.

Unlike Kif1a RNAi, Nup153 RNAi induced cell cycle progression defects in RGP cells, arresting them in the G1 phase. This aligns with findings in hepatocellular carcinoma (HCC) cells,[30] where NUP153 negatively regulates $P15^{INK4b}$ (cyclin-dependent kinase inhibitor 2B) expression,[30] thereby triggering G1/S-phase arrest.[41,42] Our results indicate that Nup153's regulation of basal INM, occurring during G1, ensures a proper sequence between basal nuclear migration and the G1/S transition.

Importantly, Nup153 RNAi also caused an accumulation of postmitotic neurons in the SVZ of developing rat brains. We observed Kif1a localization at the NE in both RGP cells and postmitotic neurons, suggesting Nup153's involvement in postmitotic neuronal migration as well. While Kif1a RNAi exerts both cell-autonomous and non-cell-autonomous effects on postmitotic neuronal migration,[11,43] Nup153 RNAi only phenocopies the cell-autonomous aspect.

To further confirm Nup153's role in RGP cell behavior, we expressed constructs of the Nup153-N, Nup153-C, and full-length Nup153 in RGP cells using *in utero* electroporation. Consistent with Nup153 RNAi results, Nup153-N expression inhibited basal INM and decorated RGP nuclei, suggesting competition with endogenous Nup153 for NPC incorporation. These results indicate that the Nup153-N localizes to the NE but cannot bind Kif1a, thereby failing to support nuclear migration.

Role of Nup153 as an NE anchor for Kif1a

We showed that the Kif1a tail domain localizes to the NE in both neuronal and nonneuronal cells. Our findings demonstrate that the nucleoporin Nup153 is necessary for Kif1a NE localization in nonneuronal cells, suggesting that the NPC serves as Kif1a cargo. Nup153, located in the nuclear basket structure on the nucleoplasmic side of the NPC, uses its C-terminal domain, which is characterized by high flexibility and mobility, to associate with Kif1a.

Nup153 domain organization

Nup153 (UniProt: P49790) is a 1,475-residue protein (~154 kDa) comprising three domains: an N-terminal pore targeting region, a central domain with zinc-finger motifs, and a C-terminal phenylalanine-glycine (FG)-repeat domain. The C terminus of Nup153, rich in degenerate pentapeptide repeats,[44] is natively unfolded.

Nup153 localization

Early studies using immuno-gold electron microscopy positioned Nup153 primarily on the nuclear basket of the NPC.[45] Subsequent studies revealed more complicated localization patterns, showing different Nup153 epitopes exposed at various regions of the nuclear pore basket.[35,46–49] The zinc-finger region is

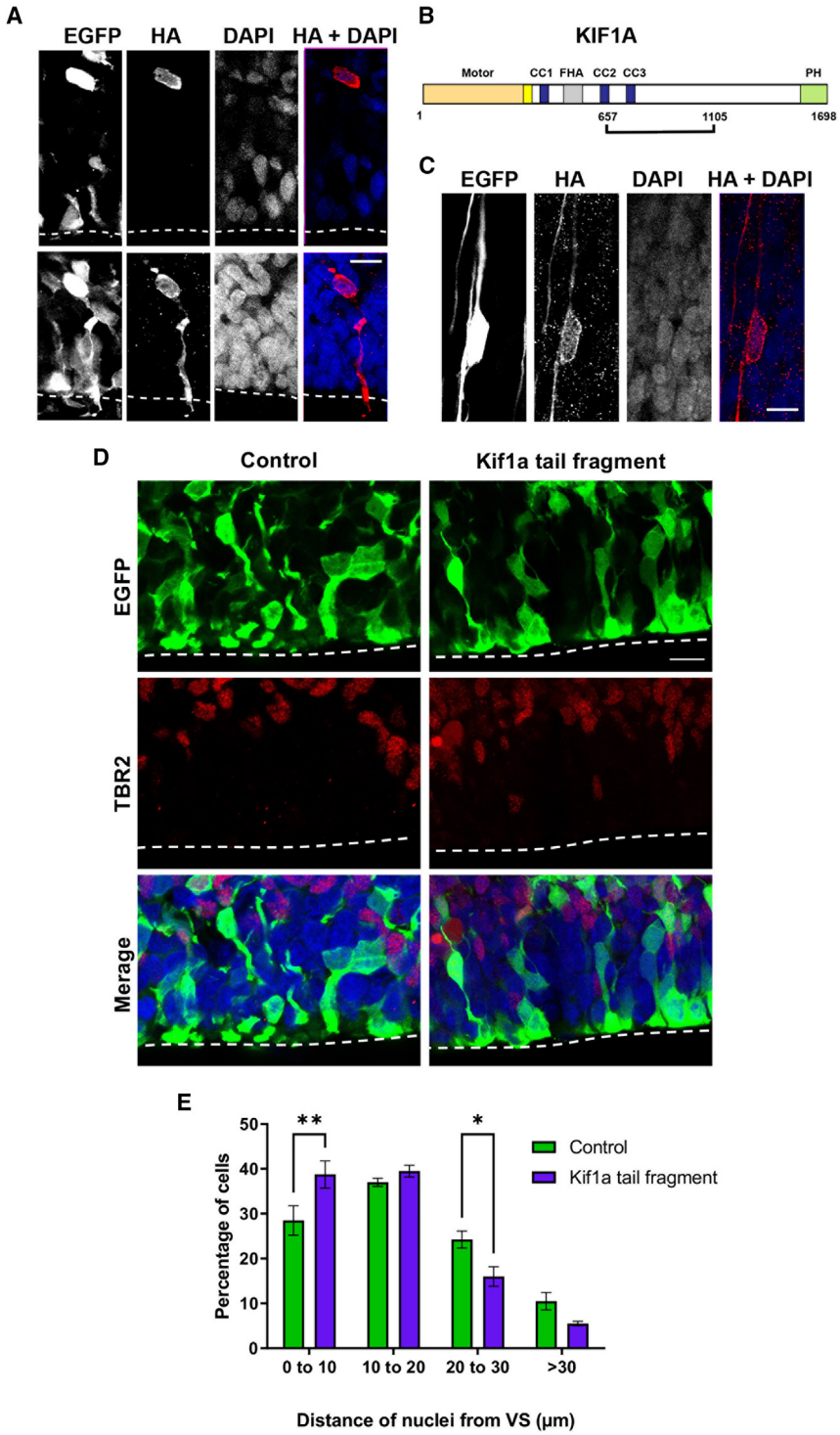

Figure 6. KIF1A tail fragment decorates NE in RGP cells and migrating neurons, and its expression in RGP cells inhibits basal INM

(A, C, and D) E16 embryonic brains were *in utero* electroporated with the KIF1A tail fragment with HA tag that is fused at its N terminus and EGFP tag that is cytoplasmic and subsequently imaged following fixation 3 days post-injection at E19.

(A) Fixed images of the ventricular zone (VZ) from the electroporated brains stained for EGFP and HA. Dashed lines represent the VS. HA staining showed cleared NE decoration in a subset of RGP cells. Scale bar: 10 μm.

(B) Schematic representation of the KIF1A molecule and its tail fragment that was used in this study.

(C) Fixed images of the cortical plate region from the electroporated brains stained for EGFP and HA. HA staining showed cleared NE decoration in a subset of migrating neurons. Scale bar: 10 μm.

(D) Fixed images of the VZ from the electroporated brains stained for EGFP to enhance the signal and for Tbr2 to exclude intermediate precursors from the analysis. Scale bar: 10 mm.

(E) Quantification of the fixed images of the VZ from electroporated brains expressing either KIF1A tail fragment or control empty vector, representing the distance between the RGP nuclei and the VS between the two conditions. Control nuclei were distributed at a range of distances from the ventricular surface. Nuclei of KIF1A tail fragment-expressing cells accumulated relatively closer to the VS ($n = 4$ per condition; $p = 0.01$, $^{**}p < 0.01$, and $^{***}p < 0.001$; error bars = SEM).

most exposed at the distal ring, whereas the N-terminal region is closer to the membrane, presumably on the proximal ring. Nup153 may adopt an extended structure or exist in two populations with distinct regions exposed.[35,50]

Immuno-gold-labeled antibodies recognizing the C-terminal, FG-rich region of Nup153 decorate both proximal and distal regions of the nuclear pore basket and extend to cytoplasmic features of the pore.[35] Epitope-tagged Nup153 confirmed the C-terminal region's flexibility, showing it in a spread distribution within the basket and, again, on the cytoplasmic side.[35] These results suggest that the C-terminal region is flexible and is not folded into a structure that is constrained to a fixed point within the pore. Consistent with this, biophysical measurements of several FG-rich domains have led to the proposal that these regions are natively unfolded and exist in equilibrium between many conformations.[44] These lines of investigation suggest that the C-terminal region can extend to the cytoplasmic face of the NPC, allowing interaction with cytoplasmic proteins such as Kif1a.

There is precedence for other cytoplasmic proteins, such as DICER1, interacting with Nup153,[51] detected predominantly in the cytoplasm and at the nuclear periphery via proximity ligation assay (PLA). Similarly, Nup358 interacts with BicD2 through its disordered region, recruiting dynein machinery to position the nucleus. Our data suggest that the disordered

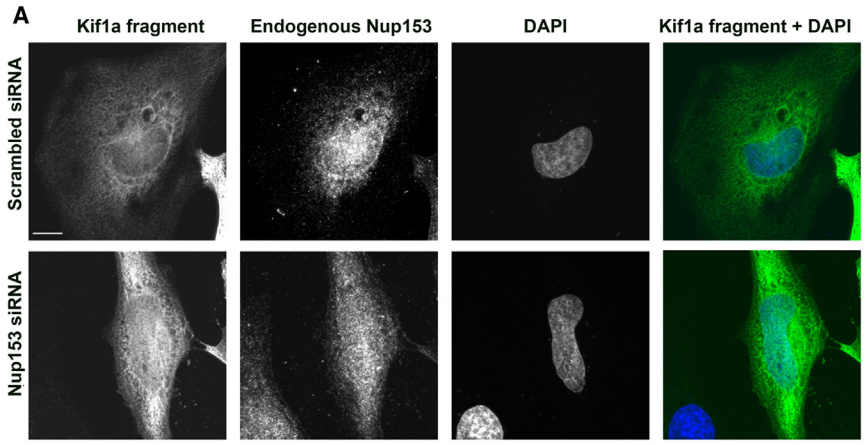

Figure 7. Nup153 is required for HeLa cell NE Kif1a recruitment

(A) HeLa cells were transfected with either Nup153 siRNA or scrambled siRNA and fixed after 48 h. 20 h prior to fixation, the cells in both the groups were also transfected with the EGFP-tagged KIF1A tail fragment. Following fixation, the cells were stained with anti-Nup153 antibody as well as anti-EGFP antibody. Nup153 siRNA-mediated loss of endogenous Nup153 (as determined by antibody staining) also led to the loss of NE decoration by KIF1A tail fragment. Scale bar: 10 μm.

(B) Quantification of NE decoration by KIF1A tail fragment in the scrambled siRNA and Nup153 siRNA groups. The experiment was reproduced three independent times (over 50 cells per condition and per experiment were counted; $^{**}p < 0.01$ and $^{***}p < 0.001$; error bars = SEM).

C-terminal region of Nup153 can stably interact with Kif1a to position the nucleus, akin to how Nup358 recruits dynein machinery through BicD2.[15] Recent studies show that a minimal domain of Nup358[52,53] activates dynein/dynactin/BicD2 for processive motility[54] on MTs, with core residues comprising disordered regions.[55]

NE decoration by Kif1a

Full-length Kif1a is autoinhibited,[56,57] which may explain the diffuse cytoplasmic distribution when overexpressed, whereas the shorter Kif1a tail domain yields NE localization. This nuclear-pore-mediated Kif1a recruitment pathway is supported by its localization at the NE in RGP cells, postmitotic neurons, and HeLa cells, which is lost upon Nup153 depletion. The high levels of soluble and vesicular Kif1a in the cytoplasm complicate its localization analysis, especially in brain tissue lacking useful G1 markers. However, Kif1a localization at the RGP NE provides the *in situ* evidence for Kif1a localization at this site.

Limitations of the study

This study provides insight into how Kif1a is anchored to the NE of RGP cells to drive INM, based on its interaction with Nup153. However, corroborating biochemical evidence was not obtained due to technical limitations. Additionally, while our data indicate that both basal INM occurring during G1 phase and G1/S transition in RGP cells are regulated by Nup153, the precise mechanism of cell cycle control of basal INM remains to be elucidated. We also acknowledge that we did not conduct any genetic studies to more cleanly assess the role of Nup153 in embryonic brain development due to the lack of easily available Nup153 knockout mouse models,[58] although rats have been the leading model organisms used in neuroscience research for years and offer practical advantages, especially when it comes to surgical procedures, owing to their large size.[59] Finally, we used only one shRNA for our Nup153 KD experiments, although it is ideal to use two different constructs to provide more robust validation.

RESOURCE AVAILABILITY

Lead contact

Further information and requests for resources and reagents should be directed to and will be fulfilled by the lead contact, Aditi Falnikar (aditi.falnikar@gmail.com).

Materials availability

Plasmids generated in this study are available from the lead contact.

Data and code availability

- This study did not generate any unique datasets.
- This study did not report original code.
- The source data that support the findings of this study are available from the lead contact upon reasonable request.

ACKNOWLEDGMENTS

The authors thank Dr. Sozanne R. Solmaz at Binghamton University for critically reading and providing input on this manuscript. This work was supported by grant R01 NS114636-01 to R.B.V. and an Irving Institute for Clinical and Translational Research Pilot Award to A.F.

AUTHOR CONTRIBUTIONS

A.F. and R.B.V. conceived the project. A.F. designed and performed most of the experiments, analyzed and interpreted all the data, and prepared figures. R.B.V. and A.F. wrote the original draft of the manuscript. S.Q. performed western blots and additional biochemical experiments. H.-J.Z. and H.-Y.C. performed western blots and *in utero* electroporation experiments for the

revision, which were supervised by J.-W.T. S.Q. helped with experimental design and interpretation of data. R.B.V. supervised the project.

DECLARATION OF INTERESTS

The authors declare no competing interests.

STAR★METHODS

Detailed methods are provided in the online version of this paper and include the following:

- KEY RESOURCES TABLE
- EXPERIMENTAL MODEL AND STUDY PARTICIPANT DETAILS
  - Ethics statement
  - Animals
  - Cell culture
- METHOD DETAILS
  - In utero electroporation
  - Immunohistochemistry and live imaging
  - RNAi and constructs
  - Western blot
  - Imaging
- QUANTIFICATION AND STATISTICAL ANALYSIS

SUPPLEMENTAL INFORMATION

Supplemental information can be found online at https://doi.org/10.1016/j.celrep.2024.115008.

Received: October 12, 2023
Revised: October 14, 2024
Accepted: November 7, 2024
Published: December 11, 2024

REFERENCES

1. Götz, M., and Huttner, W.B. (2005). The cell biology of neurogenesis. Nat. Rev. Mol. Cell Biol. *6*, 777–788. https://doi.org/10.1038/nrm1739.
2. Kriegstein, A., and Alvarez-Buylla, A. (2009). The glial nature of embryonic and adult neural stem cells. Annu. Rev. Neurosci. *32*, 149–184. https://doi.org/10.1146/annurev.neuro.051508.135600.
3. Noctor, S.C., Flint, A.C., Weissman, T.A., Dammerman, R.S., and Kriegstein, A.R. (2001). Neurons derived from radial glial cells establish radial units in neocortex. Nature *409*, 714–720. https://doi.org/10.1038/35055553.
4. Rakic, P. (1988). Specification of cerebral cortical areas. Science *241*, 170–176. https://doi.org/10.1126/science.3291116.
5. Taverna, E., and Huttner, W.B. (2010). Neural progenitor nuclei IN motion. Neuron *67*, 906–914. https://doi.org/10.1016/j.neuron.2010.08.027.
6. Hu, D.J.K., Baffet, A.D., Nayak, T., Akhmanova, A., Doye, V., and Vallee, R.B. (2013). Dynein recruitment to nuclear pores activates apical nuclear migration and mitotic entry in brain progenitor cells. Cell *154*, 1300–1313. https://doi.org/10.1016/j.cell.2013.08.024.
7. Tsai, J.W., Lian, W.N., Kemal, S., Kriegstein, A.R., and Vallee, R.B. (2010). Kinesin 3 and cytoplasmic dynein mediate interkinetic nuclear migration in neural stem cells. Nat. Neurosci. *13*, 1463–1471. https://doi.org/10.1038/nn.2665.
8. Kosodo, Y. (2012). Interkinetic nuclear migration: beyond a hallmark of neurogenesis. Cell. Mol. Life Sci. *69*, 2727–2738. https://doi.org/10.1007/s00018-012-0952-2.
9. Tsai, J.W., Chen, Y., Kriegstein, A.R., and Vallee, R.B. (2005). LIS1 RNA interference blocks neural stem cell division, morphogenesis, and motility at multiple stages. J. Cell Biol. *170*, 935–945. https://doi.org/10.1083/jcb.200505166.
10. Spear, P.C., and Erickson, C.A. (2012). Interkinetic nuclear migration: a mysterious process in search of a function. Dev. Growth Differ. *54*, 306–316. https://doi.org/10.1111/j.1440-169X.2012.01342.x.
11. Carabalona, A., Hu, D.J.K., and Vallee, R.B. (2016). KIF1A inhibition immortalizes brain stem cells but blocks BDNF-mediated neuronal migration. Nat. Neurosci. *19*, 253–262. https://doi.org/10.1038/nn.4213.
12. Del Bene, F., Wehman, A.M., Link, B.A., and Baier, H. (2008). Regulation of neurogenesis by interkinetic nuclear migration through an apical-basal notch gradient. Cell *134*, 1055–1065. https://doi.org/10.1016/j.cell.2008.07.017.
13. Tsai, J.W., Bremner, K.H., and Vallee, R.B. (2007). Dual subcellular roles for LIS1 and dynein in radial neuronal migration in live brain tissue. Nat. Neurosci. *10*, 970–979. https://doi.org/10.1038/nn1934.
14. Splinter, D., Razafsky, D.S., Schlager, M.A., Serra-Marques, A., Grigoriev, I., Demmers, J., Keijzer, N., Jiang, K., Poser, I., Hyman, A.A., et al. (2012). BICD2, dynactin, and LIS1 cooperate in regulating dynein recruitment to cellular structures. Mol. Biol. Cell *23*, 4226–4241. https://doi.org/10.1091/mbc.E12-03-0210.
15. Splinter, D., Tanenbaum, M.E., Lindqvist, A., Jaarsma, D., Flotho, A., Yu, K.L., Grigoriev, I., Engelsma, D., Haasdijk, E.D., Keijzer, N., et al. (2010). Bicaudal D2, dynein, and kinesin-1 associate with nuclear pore complexes and regulate centrosome and nuclear positioning during mitotic entry. PLoS Biol. *8*, e1000350. https://doi.org/10.1371/journal.pbio.1000350.
16. Bolhy, S., Bouhlel, I., Dultz, E., Nayak, T., Zuccolo, M., Gatti, X., Vallee, R., Ellenberg, J., and Doye, V. (2011). A Nup133-dependent NPC-anchored network tethers centrosomes to the nuclear envelope in prophase. J. Cell Biol. *192*, 855–871. https://doi.org/10.1083/jcb.201007118.
17. Niwa, S., Lipton, D.M., Morikawa, M., Zhao, C., Hirokawa, N., Lu, H., and Shen, K. (2016). Autoinhibition of a Neuronal Kinesin UNC-104/KIF1A Regulates the Size and Density of Synapses. Cell Rep. *16*, 2129–2141. https://doi.org/10.1016/j.celrep.2016.07.043.
18. Okada, Y., Yamazaki, H., Sekine-Aizawa, Y., and Hirokawa, N. (1995). The neuron-specific kinesin superfamily protein KIF1A is a unique monomeric motor for anterograde axonal transport of synaptic vesicle precursors. Cell *81*, 769–780. https://doi.org/10.1016/0092-8674(95)90538-3.
19. Yonekawa, Y., Harada, A., Okada, Y., Funakoshi, T., Kanai, Y., Takei, Y., Terada, S., Noda, T., and Hirokawa, N. (1998). Defect in synaptic vesicle precursor transport and neuronal cell death in KIF1A motor protein-deficient mice. J. Cell Biol. *141*, 431–441. https://doi.org/10.1083/jcb.141.2.431.
20. Zahn, T.R., Angleson, J.K., MacMorris, M.A., Domke, E., Hutton, J.F., Schwartz, C., and Hutton, J.C. (2004). Dense core vesicle dynamics in Caenorhabditis elegans neurons and the role of kinesin UNC-104. Traffic *5*, 544–559. https://doi.org/10.1111/j.1600-0854.2004.00195.x.
21. Lo, K.Y., Kuzmin, A., Unger, S.M., Petersen, J.D., and Silverman, M.A. (2011). KIF1A is the primary anterograde motor protein required for the axonal transport of dense-core vesicles in cultured hippocampal neurons. Neurosci. Lett. *491*, 168–173. https://doi.org/10.1016/j.neulet.2011.01.018.
22. Tanaka, Y., Niwa, S., Dong, M., Farkhondeh, A., Wang, L., Zhou, R., and Hirokawa, N. (2016). The Molecular Motor KIF1A Transports the TrkA Neurotrophin Receptor and Is Essential for Sensory Neuron Survival and Function. Neuron *90*, 1215–1229. https://doi.org/10.1016/j.neuron.2016.05.002.
23. Stavoe, A.K.H., Hill, S.E., Hall, D.H., and Colón-Ramos, D.A. (2016). KIF1A/UNC-104 Transports ATG-9 to Regulate Neurodevelopment and Autophagy at Synapses. Dev. Cell *38*, 171–185. https://doi.org/10.1016/j.devcel.2016.06.012.
24. Hung, C.O.Y., and Coleman, M.P. (2016). KIF1A mediates axonal transport of BACE1 and identification of independently moving cargoes in living SCG neurons. Traffic *17*, 1155–1167. https://doi.org/10.1111/tra.12428.

25. Chiba, K., Kita, T., Anazawa, Y., and Niwa, S. (2023). Insight into the regulation of axonal transport from the study of KIF1A-associated neurological disorder. J. Cell Sci. *136*, jcs260742. https://doi.org/10.1242/jcs.260742.

26. Boyle, L., Rao, L., Kaur, S., Fan, X., Mebane, C., Hamm, L., Thornton, A., Ahrendsen, J.T., Anderson, M.P., Christodoulou, J., et al. (2021). Genotype and defects in microtubule-based motility correlate with clinical severity in KIF1A-associated neurological disorder. HGG Adv. *2*, 100026. https://doi.org/10.1016/j.xhgg.2021.100026.

27. Stucchi, R., Plucinska, G., Hummel, J.J.A., Zahavi, E.E., Guerra San Juan, I., Klykov, O., Scheltema, R.A., Altelaar, A.F.M., and Hoogenraad, C.C. (2018). Regulation of KIF1A-Driven Dense Core Vesicle Transport: Ca(2+)/CaM Controls DCV Binding and Liprin-alpha/TANC2 Recruits DCVs to Postsynaptic Sites. Cell Rep. *24*, 685–700. https://doi.org/10.1016/j.celrep.2018.06.071.

28. Lussi, Y.C., Shumaker, D.K., Shimi, T., and Fahrenkrog, B. (2010). The nucleoporin Nup153 affects spindle checkpoint activity due to an association with Mad1. Nucleus *1*, 71–84. https://doi.org/10.4161/nucl.1.1.10244.

29. Mackay, D.R., Elgort, S.W., and Ullman, K.S. (2009). The nucleoporin Nup153 has separable roles in both early mitotic progression and the resolution of mitosis. Mol. Biol. Cell *20*, 1652–1660. https://doi.org/10.1091/mbc.e08-08-0883.

30. Gan, C., Zhou, K., Li, M., Shang, J., Liu, L., and Zhao, Q. (2022). NUP153 promotes HCC cells proliferation via c-Myc-mediated downregulation of P15(INK4b). Dig. Liver Dis. *54*, 1706–1715. https://doi.org/10.1016/j.dld.2022.02.008.

31. Zhou, L., and Panté, N. (2010). The nucleoporin Nup153 maintains nuclear envelope architecture and is required for cell migration in tumor cells. FEBS Lett. *584*, 3013–3020. https://doi.org/10.1016/j.febslet.2010.05.038.

32. Duheron, V., Chatel, G., Sauder, U., Oliveri, V., and Fahrenkrog, B. (2014). Structural characterization of altered nucleoporin Nup153 expression in human cells by thin-section electron microscopy. Nucleus *5*, 601–612. https://doi.org/10.4161/19491034.2014.990853.

33. Bastos, R., Lin, A., Enarson, M., and Burke, B. (1996). Targeting and function in mRNA export of nuclear pore complex protein Nup153. J. Cell Biol. *134*, 1141–1156. https://doi.org/10.1083/jcb.134.5.1141.

34. Enarson, P., Enarson, M., Bastos, R., and Burke, B. (1998). Amino-terminal sequences that direct nucleoporin nup153 to the inner surface of the nuclear envelope. Chromosoma *107*, 228–236. https://doi.org/10.1007/s004120050301.

35. Fahrenkrog, B., Maco, B., Fager, A.M., Köser, J., Sauder, U., Ullman, K.S., and Aebi, U. (2002). Domain-specific antibodies reveal multiple-site topology of Nup153 within the nuclear pore complex. J. Struct. Biol. *140*, 254–267. https://doi.org/10.1016/s1047-8477(02)00524-5.

36. Paulillo, S.M., Phillips, E.M., Köser, J., Sauder, U., Ullman, K.S., Powers, M.A., and Fahrenkrog, B. (2005). Nucleoporin domain topology is linked to the transport status of the nuclear pore complex. J. Mol. Biol. *351*, 784–798. https://doi.org/10.1016/j.jmb.2005.06.034.

37. Paulillo, S.M., Powers, M.A., Ullman, K.S., and Fahrenkrog, B. (2006). Changes in nucleoporin domain topology in response to chemical effectors. J. Mol. Biol. *363*, 39–50. https://doi.org/10.1016/j.jmb.2006.08.021.

38. Liu, J.S., Schubert, C.R., Fu, X., Fourniol, F.J., Jaiswal, J.K., Houdusse, A., Stultz, C.M., Moores, C.A., and Walsh, C.A. (2012). Molecular basis for specific regulation of neuronal kinesin-3 motors by doublecortin family proteins. Mol. Cell *47*, 707–721. https://doi.org/10.1016/j.molcel.2012.06.025.

39. Andero, R., Heldt, S.A., Ye, K., Liu, X., Armario, A., and Ressler, K.J. (2011). Effect of 7,8-dihydroxyflavone, a small-molecule TrkB agonist, on emotional learning. Am. J. Psychiatry *168*, 163–172. https://doi.org/10.1176/appi.ajp.2010.10030326.

40. Englund, C., Fink, A., Lau, C., Pham, D., Daza, R.A.M., Bulfone, A., Kowalczyk, T., and Hevner, R.F. (2005). Pax6, Tbr2, and Tbr1 are expressed sequentially by radial glia, intermediate progenitor cells, and postmitotic neurons in developing neocortex. J. Neurosci. *25*, 247–251. https://doi.org/10.1523/JNEUROSCI.2899-04.2005.

41. Hannon, G.J., and Beach, D. (1994). p15INK4B is a potential effector of TGF-beta-induced cell cycle arrest. Nature *371*, 257–261. https://doi.org/10.1038/371257a0.

42. Yaginuma, Y., Hayashi, H., Kawai, K., Kurakane, T., Saitoh, Y., Kitamura, S., Sengoku, K., and Ishikawa, M. (1997). Analysis of the Rb gene and cyclin-dependent kinase 4 inhibitor genes (p16INK4 and p15INK4B) in human ovarian carcinoma cell lines. Exp. Cell Res. *233*, 233–239. https://doi.org/10.1006/excr.1997.3560.

43. Polleux, F., Whitford, K.L., Dijkhuizen, P.A., Vitalis, T., and Ghosh, A. (2002). Control of cortical interneuron migration by neurotrophins and PI3-kinase signaling. Development *129*, 3147–3160. https://doi.org/10.1242/dev.129.13.3147.

44. Denning, D.P., Patel, S.S., Uversky, V., Fink, A.L., and Rexach, M. (2003). Disorder in the nuclear pore complex: the FG repeat regions of nucleoporins are natively unfolded. Proc. Natl. Acad. Sci. USA *100*, 2450–2455. https://doi.org/10.1073/pnas.0437902100.

45. Sukegawa, J., and Blobel, G. (1993). A nuclear pore complex protein that contains zinc finger motifs, binds DNA, and faces the nucleoplasm. Cell *72*, 29–38. https://doi.org/10.1016/0092-8674(93)90047-t.

46. Krull, S., Thyberg, J., Björkroth, B., Rackwitz, H.R., and Cordes, V.C. (2004). Nucleoporins as components of the nuclear pore complex core structure and Tpr as the architectural element of the nuclear basket. Mol. Biol. Cell *15*, 4261–4277. https://doi.org/10.1091/mbc.e04-03-0165.

47. Pante, N., Bastos, R., McMorrow, I., Burke, B., and Aebi, U. (1994). Interactions and three-dimensional localization of a group of nuclear pore complex proteins. J. Cell Biol. *126*, 603–617. https://doi.org/10.1083/jcb.126.3.603.

48. Pante, N., Thomas, F., Aebi, U., Burke, B., and Bastos, R. (2000). Recombinant Nup153 incorporates in vivo into Xenopus oocyte nuclear pore complexes. J. Struct. Biol. *129*, 306–312. https://doi.org/10.1006/jsbi.2000.4232.

49. Walther, T.C., Fornerod, M., Pickersgill, H., Goldberg, M., Allen, T.D., and Mattaj, I.W. (2001). The nucleoporin Nup153 is required for nuclear pore basket formation, nuclear pore complex anchoring and import of a subset of nuclear proteins. EMBO J. *20*, 5703–5714. https://doi.org/10.1093/emboj/20.20.5703.

50. Fahrenkrog, B., and Aebi, U. (2003). The nuclear pore complex: nucleocytoplasmic transport and beyond. Nat. Rev. Mol. Cell Biol. *4*, 757–766. https://doi.org/10.1038/nrm1230.

51. Ando, Y., Tomaru, Y., Morinaga, A., Burroughs, A.M., Kawaji, H., Kubosaki, A., Kimura, R., Tagata, M., Ino, Y., Hirano, H., et al. (2011). Nuclear pore complex protein mediated nuclear localization of dicer protein in human cells. PLoS One *6*, e23385. https://doi.org/10.1371/journal.pone.0023385.

52. Noell, C.R., Loh, J.Y., Debler, E.W., Loftus, K.M., Cui, H., Russ, B.B., Zhang, K., Goyal, P., and Solmaz, S.R. (2019). Role of Coiled-Coil Registry Shifts in the Activation of Human Bicaudal D2 for Dynein Recruitment upon Cargo Binding. J. Phys. Chem. Lett. *10*, 4362–4367. https://doi.org/10.1021/acs.jpclett.9b01865.

53. Cui, H., Noell, C.R., Behler, R.P., Zahn, J.B., Terry, L.R., Russ, B.B., and Solmaz, S.R. (2019). Adapter Proteins for Opposing Motors Interact Simultaneously with Nuclear Pore Protein Nup358. Biochemistry *58*, 5085–5097. https://doi.org/10.1021/acs.biochem.9b00907.

54. Gibson, J.M., Cui, H., Ali, M.Y., Zhao, X., Debler, E.W., Zhao, J., Trybus, K.M., Solmaz, S.R., and Wang, C. (2022). Coil-to-alpha-helix transition at the Nup358-BicD2 interface activates BicD2 for dynein recruitment. Elife *11*, e74714. https://doi.org/10.7554/eLife.74714.

55. Bley, C.J., Nie, S., Mobbs, G.W., Petrovic, S., Gres, A.T., Liu, X., Mukherjee, S., Harvey, S., Huber, F.M., Lin, D.H., et al. (2022). Architecture of the

cytoplasmic face of the nuclear pore. Science *376*, eabm9129. https://doi.org/10.1126/science.abm9129.

56. Hammond, J.W., Cai, D., Blasius, T.L., Li, Z., Jiang, Y., Jih, G.T., Meyhofer, E., and Verhey, K.J. (2009). Mammalian Kinesin-3 motors are dimeric in vivo and move by processive motility upon release of autoinhibition. PLoS Biol. *7*, e72. https://doi.org/10.1371/journal.pbio.1000072.

57. Gabrych, D.R., Lau, V.Z., Niwa, S., and Silverman, M.A. (2019). Going Too Far Is the Same as Falling Short(dagger): Kinesin-3 Family Members in Hereditary Spastic Paraplegia. Front. Cell. Neurosci. *13*, 419. https://doi.org/10.3389/fncel.2019.00419.

58. https://en.gempharmatech.com/product/details100035_3699724.html.

59. Ellenbroek, B., and Youn, J. (2016). Rodent models in neuroscience research: is it a rat race? Dis. Model. Mech. *9*, 1079–1087. https://doi.org/10.1242/dmm.026120.

60. Baffet, A.D., Hu, D.J., and Vallee, R.B. (2015). Cdk1 Activates Pre-mitotic Nuclear Envelope Dynein Recruitment and Apical Nuclear Migration in Neural Stem Cells. Dev. Cell *33*, 703–716. https://doi.org/10.1016/j.devcel.2015.04.022.

STAR★METHODS

KEY RESOURCES TABLE

REAGENT or RESOURCE	SOURCE	IDENTIFIER
Antibodies		
Rabbit polyclonal Tbr2	Millipore	Cat# AB2283, RRID:AB_10806889
Rabbit polyclonal Ki67	Millipore	Cat# AB9260, RRID:AB_2142366
Rabbit monoclonal CyclinD1	Thermo Scientific	Cat# RM-9104-S0, RRID:AB_149914
Mouse monoclonal phosphor-histone H3	Abcam	Cat# ab14955, RRID:AB_443110
Rat monoclonal BrDU	Abcam	Cat# ab6326, RRID:AB_2313786
Rabbit monoclonal Kif1a	Abcam	Cat.# Ab240222
Rabbit polyclonal HA	Sigma-Aldrich	Cat# H6908, RRID:AB_260070
Mouse monoclonal mCherry	Abcam	Cat# ab167453, RRID:AB_2571870
Mouse monoclonal EGFP	Abcam	Cat# ab1218, RRID:AB_298911
Rabbit polyclonal EGFP	Invitrogen	Cat# 11122, RRID: AB_3668879
Rabbit polyclonal NeuN	Sigma-Aldrich	Cat# SAB4300883, RRID: AB_3668883
Rabbit polyclonal Tbr1	Abcam	Cat# ab31940, RRID:AB_2200219
Chemicals, peptides, and recombinant proteins		
Aqua-Poly mounting media	Polysciences	Cat#18606
Low melting agarose	IBI Scientific	Cat#70057
Penicillin/streptomycin/glutamine	Life Technologies	Cat#10378-016
Agarose	Sigma	Cat#9539
Normal Donkey Serum	Sigma	Cat#9663
Hanks balanced salt solution	Life Technologies	Cat#24020-117
Basal MEM	Life Technologies	Cat#21010-046
Horse serum	Life Technologies	Cat#26050-088
Glucose	Sigma	Cat#5767
Dye	Sigma	Cat#7252
Experimental models: Cell lines		
HeLa	Gift of Dr. Allan, Univ of Manchester	HELAM
C6 Rat Glioma cells	ATCC	CCL-107
Experimental models: Organisms/strains		
Sprague Dawley Pregnant Rats	Taconic	NA
Recombinant DNA		
pCAGIG vector	Addgene	Cat#11159
pCAGIG-HA-Nup153-IRES-EGFP	This paper	NA
pCAGIG-HA-Nup153-N-IRES-EGFP	This paper	NA
pCAGIG-HA-Nup153-C-IRES-EGFP	This paper	NA
pCAGIG-HA-Kif1a (657–1105)-IRES-EGFP	This paper	NA
pRNAT-U6.1/*Neo* Nup153 shRNA	This paper	NA
pRNAT-U6.1/*Neo* Nup153 scrambled shRNA	This paper	NA
pRNAT-U6.1/*Neo* Nup160 shRNA	This paper	NA
pCAGiG-HA-Nup153	This paper	NA
pCAGiG-Nup153-IRES-GFP	This paper	NA
pCMV- EGFP-Nup153-C	This paper	NA
pCMV-EGFP-Nup153-N	This paper	NA
pCMV-EGFP-Nup153	This paper	NA
pCMV-mCherry- Kif1a (657–1105)	This paper	NA
Software and algorithms		
Fiji	ImageJ	https://fiji.sc

EXPERIMENTAL MODEL AND STUDY PARTICIPANT DETAILS

Ethics statement

All the experiments were done in accordance with the animal welfare guidelines and the guidance of the Institutional Animal Care and Use Committee at Columbia University (New York, NY).

Animals

Timed Sprague Dawley pregnant rats used for *in utero* electroporation were obtained from Taconic, and were housed in Columbia University animal facilities. All the experiments conducted were done in accordance with the animal welfare guidelines and the guidance of the Institutional Animal Care and Use Committee (IACUC) at Columbia University.

Cell culture

C6 rat glioma cells (ATCC # CCL-107) and HeLa cells (a gift from Dr. Viki Allan, University of Manchester) were cultured in DMEM supplemented with 10% FBS, 1% penicillin/streptomycin and maintained at 37°C with 5% CO_2. Transfection of C6 cells or HeLa cells was performed using a nucleofector kit V (Lonza) with an Amaxa Nucleofector II set, according to the manufacturer's instructions. Cells for immunoblotting analysis were collected 72 h following transfection. Transfection of HeLa cells was performed using Effectene transfection reagent (Qiagen), according to the manufacturer's instructions. Cells were fixed 20 h following transfection, and further processed for immunostaining analysis and imaging.

METHOD DETAILS

In utero electroporation

Plasmids encoding for shRNAs or cDNA were injected into the lateral ventricles of embryonic rat brain at E16 and electroporated as described.[60] Specifically, timed pregnant Sprague Dawley E16 rats were anesthetized with a mixture of ketamine/xylazine (respectively at 90 and 5 mg/kg), administered intraperitoneally. To avoid excessive heat-loss during the surgical procedure, an external heating source was provided. For pain management, bupivacaine (2 mg/kg) was administered via a subcutaneous injection at the site of the future incision, and buprenorphine (0.05 mg/kg) was administered by a subcutaneous injection. This dose of buprenorphine was re-administered to the animal every 8–12 h, for up to 48 h following the surgery. Abdominal cavity was opened, and uterine horns were exposed and *trans*-illuminated for clear identification of the brain ventricles. For easy visualization of the DNA in the brain ventricular space, a nontoxic dye (Sigma, F7252) was added to the DNA before surgery and injected with a sharpened glass needle. After injection, plasmids were further electroporated by discharging a 4000 mF capacitor charged to 50V with a BTX ECM 830 electroporator (BTX Harvard Apparatus, Holliston, MA, USA). The voltage was discharged in five electrical pulses at 950ms intervals via 7mm electrodes placed on the head of the embryo across the uterine wall. The embryos were returned to the abdominal cavity, and the wound was closed. Rats were monitored every day after surgery.

Immunohistochemistry and live imaging

For live imaging, brains were harvested 3 days after the electroporation. The dissected rat brains were embedded in 4% low-melting agarose (IBI Scientific, IB70057) prepared in artificial cerebrospinal fluid[60] and sliced coronally (300-μm) on a vibratome (Leica microsystems). The slices were placed on 0.4μm, 30mm diameter Millicell-CM inserts (Millipore) in cortical culture medium containing 25% HBSS (Life Technologies, 24020-117), 47% basal MEM (Life Technologies, 21010-046), 25% normal horse serum (Life Technologies, 26050-088), 1% penicillin/streptomycin/glutamine (Life Technologies, 10378-016), and 2% of 30% glucose (Sigma, G5767) in a 50-mm glass-bottom dish (MatTek Corporation, P50G-0-14-F) and imaged on an IX80 laser scanning confocal microscope (Olympus FV1000 Spectral Confocal System) at intervals of 10 min for up to 24 h.

For fixed imaging, embryonic (E19 or E20) rat brains were harvested and fixed with chilled saline and 4% paraformaldehyde (PFA; EMS, w/v) and then incubated in 4% PFA overnight. Brains were then embedded in 4% of agarose (Sigma, A9539) and sliced sectioned coronally (100μm) on a vibratome (Leica microsystems). After blocking in 5% normal donkey serum (Sigma, D9663) in PBS-Triton 0.5% for 1 h, slices were incubated with primary antibodies diluted in the blocking solution, overnight on a shaker, at 4°C. Secondary antibodies (1:500) and DAPI (Thermo Scientific, 62248; 1:10,000 dilution) were diluted in PBS and incubated for 2 h at room temperature. For BrDU labeling experiments, BrDU (Sigma-Aldrich, B5002) was injected at 50 mg/kg body weight intra-peritoneally 20 min prior to embryo harvest, then, brain slices were first incubated in 2N HCl for 25 min at 37°C, and then washed in PBS prior to antibody incubation. For EdU labeling experiments, EdU (Fisher Scientific Cat# A10044) was injected at 10 mg/kg body weight intra-peritoneally 20 min prior to embryo harvest. Slices were mounted with Aqua-Poly mounting media (Polysciences, 18606).

Antibodies used in this study were: Tbr2 (Millipore, AB2283), KI67 (Millipore, AB9260), Cyclin D1 (ThermoScientific, RM-9104-S0), phospho-histone H3 (Abcam, ab14955), BrDU (Abcam, ab6326), Kif1a (Abcam, ab240222), HA (Sigma-Aldrich, H6908), mCherry (Abcam, ab167453), GFP (Abcam, ab1218) and donkey fluorophore–conjugated secondary antibodies (Jackson Labs). Nup153 antibody was a kind gift from Dr. Brian E. Burke, A*STAR Skin Research Labs (A*SRL) – Biopolis, Singapore.

RNAi and constructs

shRNA expressing constructs were designed to target internal gene sequences unique to rat Nup160 and rat Nup153, in a pRetro-U6G vector (Cellogenetics), which also expressed soluble GFP to label-transfected cells. The shRNA sequence for Nup160 was 5′-CCCTATGTGAATCTGCATAAT-3′, and the sequence for Nup153 was 5′-ACTTCAGTTTCTGGTCGCAAGATAA-3′. Scrambled Nup153 shRNA sequence was 5′-GTGCATAATATATGCGATCTATGCC-3'. Full-length human Nup153 and Nup153-C as well as Nup153-N were obtained from Addgene (Addgene, plasmid no.s #64268, #64318, #64317) and cloned into pCAGIG vector (Addgene, plasmid no. 11159). Full-length and functional domain constructs of Nup153 were HA (YPYPVPDYA). Human kif1a-tail fragment 650–1105 aa[27] was a gift from Dr. Casper Hoogenraad (Genentech).

Western blot

shRNAs and were transfected in rat C6 brain glioma cells cultured in DMEM supplemented with 10% FBS and 1% penicillin/streptomycin and maintained at 37°C with 5% CO_2. Transfection of cultured cells with shRNAs for Nup153 and Nup153 scrmabled was performed using a Lonza Nucleofector kit V and an Amaxa Nucleofector, according to the manufacturer's instructions. Cells transfected with shRNAs were collected 72 h (for shRNAs) after transfection.

Cells transfected with shRNAs and brain samples were lysed on ice in Lysis Buffer (pH 7.2, 50 mM Tris-HCl, 150 mM NaCl, 1% Triton X-100, and 0.5% deoxycholic acid buffer) containing 1 mM DTT and a protease inhibitor cocktail (Sigma, P8340). Purified lysates were loaded on a polyacrylamide gel and transferred to a polyvinylidene difluoride membrane. The membrane was blocked in PBS with 0.5% powdered milk, incubated with primary antibodies diluted in PBS with 0.1% of powder milk, and washed and incubated with secondary LI-COR antibodies in PBS. Imaging of the blots was performed using an Odyssey system (LI-COR). Antibody from Abcam (ab 24700) was used to detect Nup153 on the Western blot.

Imaging

All images were collected with an IX80 laser scanning confocal microscope (Olympus FV1000 Spectral Confocal System). Brain sections were imaged using a 60 ×1.42 NA oil objective or a 10 ×0.40 NA air objective. All images were analyzed using ImageJ software (National Institutes of Health).

QUANTIFICATION AND STATISTICAL ANALYSIS

For all experiments involving *in utero* electroporation, at least 3 embryos were collected from at least three different pregnant rats. Sample sizes are specified in figure legends. All statistical analysis was performed using Prism 6 (GraphPad Software, La Jolla, CA, USA). Unpaired *t* test (two-tailed), with Welch's correction, was used to determine significance between two groups. Definition of statistical significance was $p < 0.05$. $p < 0.05$, $p < 0.01$, $p < 0.001$ values are labeled with *, ** and ***, respectively. Error bars represent mean ± SEM (Standard Error of the Mean) unless stated otherwise.

Cell Reports, Volume *43*

Supplemental information

The nucleoporin Nup153 is the anchor for Kif1a during basal nuclear migration in brain progenitor cells

Aditi Falnikar, Sebastian Quintremil, Hung-Jun Zhao, Haw-Yuan Cheng, Paige Helmer, Jin-Wu Tsai, and Richard B. Vallee

Supplemental Figure Legends

Figure S1

Nup153 shRNA efficiently knocks down Nup153 protein expression in C6 glioma cells, Related to Figure 1.

A. Western blot showing depletion of Nup153 protein upon transfection of C6 rat glioma cells with Nup153 shRNA, but not scrambled shRNA, for 72 h., quantified in **B.** (n = 3, $**p < 0.01$; $***p < 0.001$; error bars = SEM).

C. A separate Western blot showing rescue of Nup153 protein levels upon co-transfection of C6 rat glioma cells with Nup153 shRNA, or scrambled shRNA and RNAi-insensitive human Nup153 cDNA, quantified in **D.** (n = 3, $**p < 0.01$; $***p < 0.001$; error bars = SEM).

Figure S2

Nup160 shRNA expression has no effect on nuclear movement in radial glial progenitors, Related to Figure 1.

E16 embryonic brains were in utero electroporated with either scrambled shRNA or shRNAs for Nup160 and subsequently imaged fixed 3 days post injection, at E19.

A. Fixed images of the VZ from electroporated brains stained for EGFP. Dashed line represents the VS. Nup160 RNAi had no effect on RGP somata distribution around VS. Presence of radial glial basal process indicates retention of overall cell morphology. Scale bar 15 um.

B. Quantification of distance between the RGP nuclei and the VS across the two conditions (Scramble shRNA, n = 7, Nup160 shRNA, n = 3, **p < 0.01; ***p < 0.001; ****p < 0.0001; error bars = SEM).

Figure S3

Nup153 RNAi inhibits basal INM in radial glial progenitor cells identified by Pax6 staining, Related to Figure 1.

E16 embryonic brains were in utero electroporated with either scrambled shRNA or shRNAs for Nup153 and subsequently imaged fixed 3 days post injection, at E19.

A. Fixed images of the VZ from electroporated brains stained for EGFP and Pax6. Dashed line represents the VS. KIF1A RNAi caused clear accumulation of RGP somata near VS. Pax6 staining was used to identify RGP cells. Scale bar 20 um.

B. Quantification of distance between the $Pax6^+$ RGP nuclei and the VS across the two conditions. Control nuclei were distributed at a range of distances from the ventricular surface. Nuclei of Nup153 shRNA expressing cells accumulated relatively closer to the VS. (scramble shRNA, n = 3, Nup153 shRNA, n = 3; **p < 0.01; ***p < 0.001; ****p < 0.0001; error bars = SEM).

Figure S4

Nup153 RNAi in RGP cells leads to a decrease in S phase cells, Related to Figure 2.

E16 embryonic brains were in utero electroporated with either scrambled shRNA or shRNA for Nup153. Effect of Nup153 RNAi on S phase was investigated by EdU pulse labeling. Brains were fixed at E19 and stained for EdU, and either NeuN or Tbr2.

A. Images of fixed brain sections stained with EGFP to enhance signal, EdU to label S-phase cells and NeuN to exclude postmitotic neurons from the analysis. Scale bar 100 um.

Quantification of percentage of cells that were EGFP+ as well as EdU+ but NeuN- confirmed our results that Nup153 RNAi resulted in a decrease in RGP cells in S-phase. (scramble shRNA, n = 3, Nup153 shRNA, n = 3; **p < 0.01; ***p < 0.001; ****p < 0.0001; error bars = SEM).

B. Images of VZ from the electroporated brains stained with EGFP to enhance signal, EdU to label S-phase cells and Tbr2 to exclude intermediate precursor cells from the analysis. Scale bar 10 um.

Quantification of percentage of cells that were EGFP+ as well as EdU+ but Tbr2- confirmed our results that Nup153 RNAi resulted in a decrease in RGP cells in S-phase. (scramble shRNA, n = 3, Nup153 shRNA, n = 3; **p < 0.01; ***p < 0.001; ****p < 0.0001; error bars = SEM).

Figure S5

Mechanistic insight from the Nup153 functional domains, Related to Figure 1.

A,B. E16 brains were in utero electroporated with the full-length, or the N-terminal domain or the C-terminal domain of Nup153, with HA tag fused to its N-terminus and EGFP tag that is cytoplasmic. Analysis was performed at 3 days post injection.

A. Fixed images of the VZ from the electroporated brains stained for EGFP to enhance the signal and for Tbr2 to exclude intermediate precursors from the analysis. Scale bar 10 um.

B. Quantification of the distance between RGP nuclei and the VS across the various conditions. Expression of full-length Nup153 or the Nup153-C domain alone had no detectable effect on the position of the nucleus within the RGP cells. However, Nup153-N domain expression in RGP cells caused a pronounced accumulation of most transfected cells with somata located close to the ventricular surface (n = 3 per condition; $**p < 0.01$; $***p < 0.001$; error bars = SEM).

Figure S6

Role for Nup153 in post-mitotic neuronal migration, Related to Figure 6.

E16 rat embryonic brains were in utero electroporated with shRNA for Nup153 or scrambled shRNA,. Analysis was performed 4 days post injection at E20.

A. Images of the neocortex injected with scrambled or Nup153 shRNA and stained for EGFP and Tbr1. Nup153 RNAi did not alter the distribution of $Tbr1^+$ cells. Scale bar 50 um. (n = 3 per condition)

B. Images of the neocortex injected with scrambled or Nup153 shRNA and stained for EGFP and Tbr2. Tbr2 staining was used to exclude intermediate progenitor cells during further analysis. Scale bar 100 um.

C. Quantification of the proportion of $Tbr2^-$ transfected cells in each layer of the neocortex across conditions. Depletion of Nup153 leads to an accumulation of the majority of transfected neurons at the multipolar stage within the SVZ/lower IZ. (n = 3 per condition; $**p < 0.01$; $***p < 0.001$; error bars = SEM).

Figure S7

Role of Nup153 in neuronal output during embryonic development, Related Figure 6.

E16 rat embryonic brains were in utero electroporated with shRNA for Nup153 or scrambled shRNA. Analysis was performed 4 days post injection at E20.

A. Images of the neocortex injected with scrambled or Nup153 shRNA and stained for EGFP and neuronal marker NeuN. Scale bar 100 um.

B. Quantification of the proportion of $NeuN^+$ transfected cells across the two conditions. Depletion of Nup153 leads to a decreased neuronal output in embryonic rat brains. (n = 3 per condition; $**p < 0.01$; $***p < 0.001$; error bars = SEM).

Figure S8

Nup153 is required for RGP NE Kif1a recruitment, Related to Figure 7.

A. E16 brains were in utero electroporated with one of the EGFP-tagged full-length, or the N-terminal domain or the C-terminal domain of Nup153, as well as HA tagged Kif1a tail fragment. Analysis was performed at 3 days post injection. Kif1a tail fragment showed NE decoration in cells expressing full length Nup153 or Nup153-C. Expression of Nup153-N led to loss of NE decoration by Kif1 tail fragment.

B. E16 brains were in utero electroporated with one of the EGFP tagged scrambled shRNA or Nup153 shRNA, as well as HA-tagged Kif1a tail fragment. Analysis was performed at 3 days post injection. While Kif1a NE localization was observed in scrambled shRNA expressing RGP cells, Nup153 RNAi resulted in the loss of Kif1a NE localization. Scale bar 5 um.

Supplemental Figures:

Figure S1

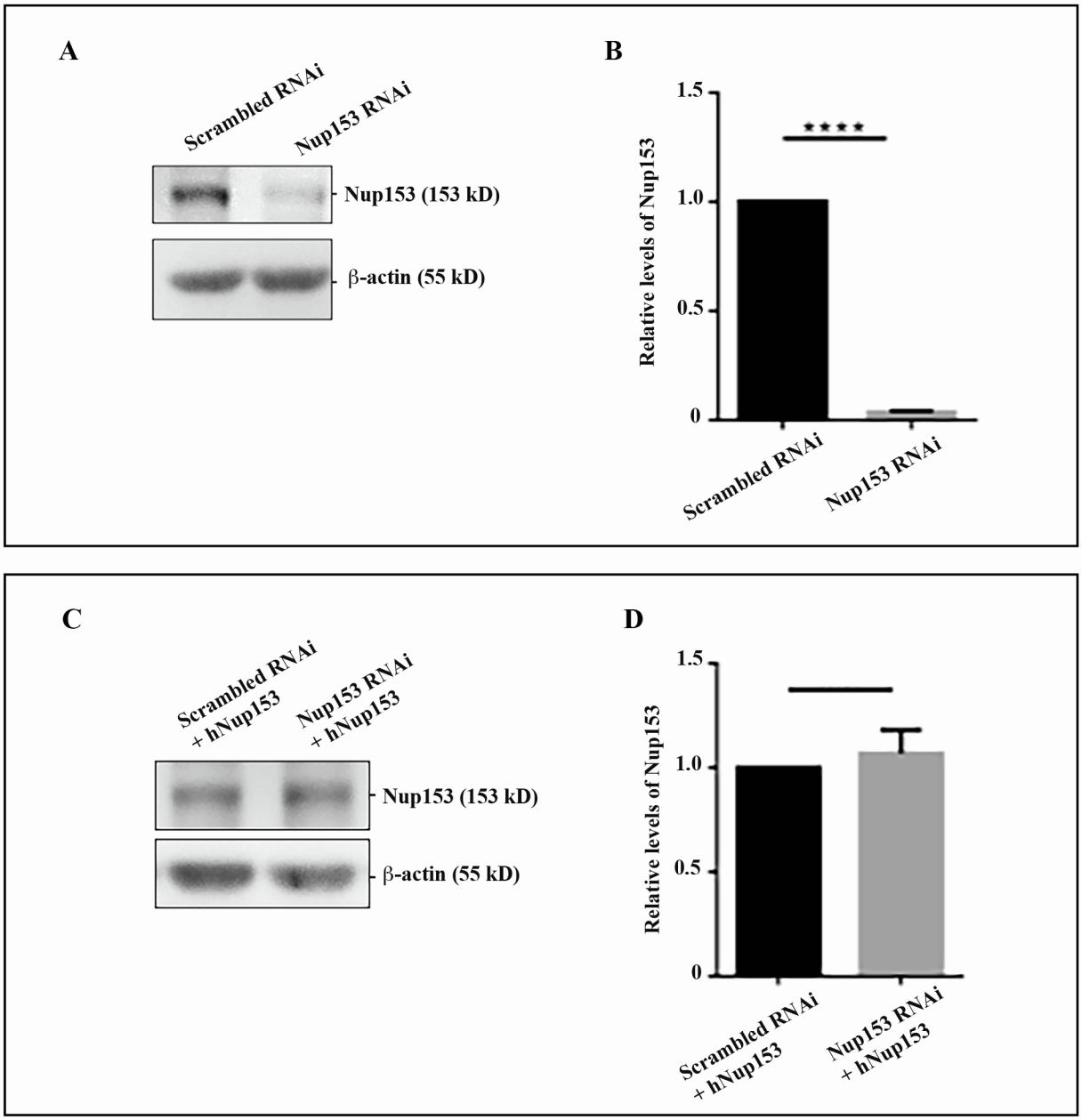

Figure S2

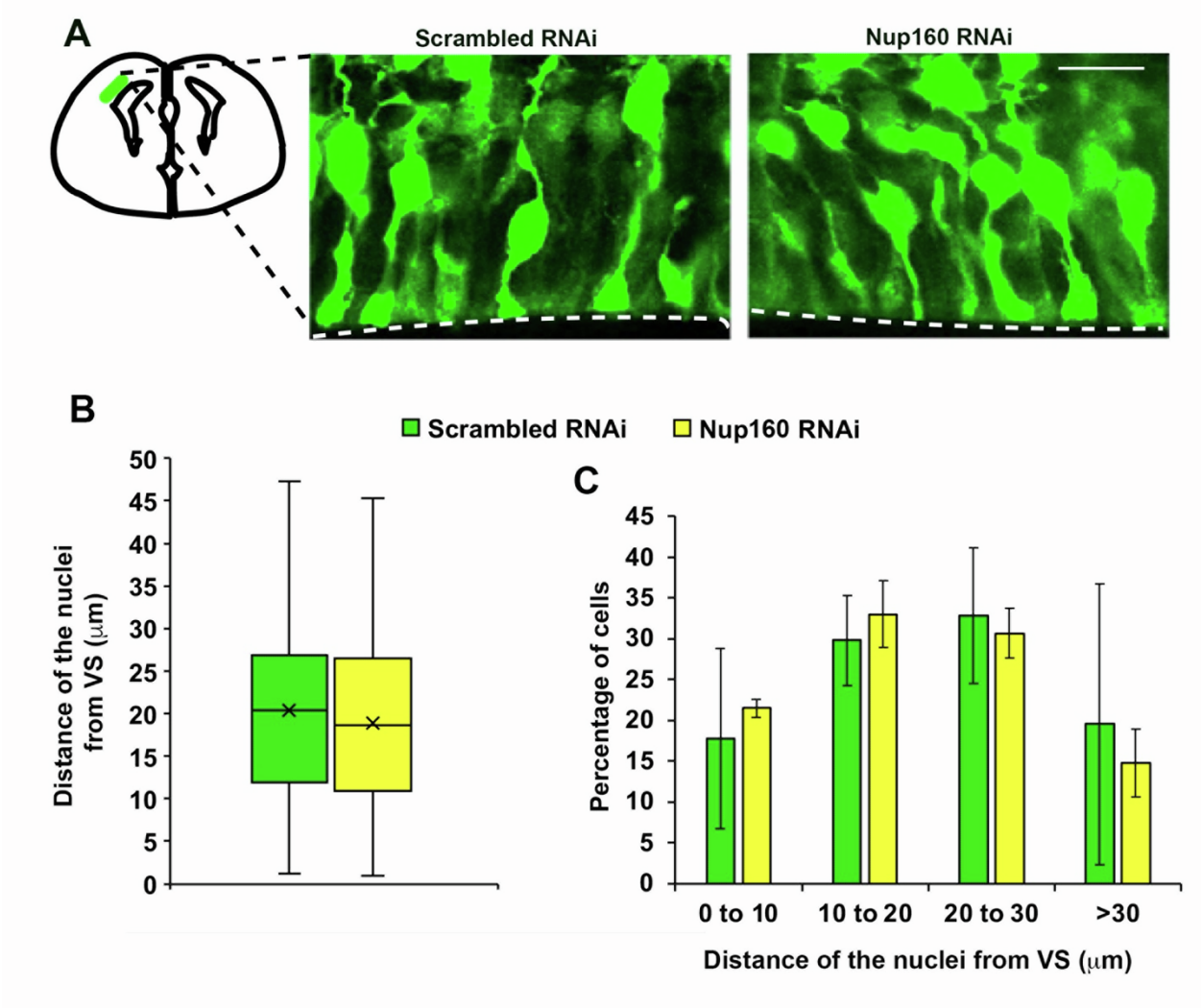
A
Scrambled RNAi
Nup160 RNAi
B
Scrambled RNAi
Nup160 RNAi
Distance of the nuclei from VS (μm)
50
45
40
35
30
25
20
15
10
5
0
C
Percentage of cells
45
40
35
30
25
20
15
10
5
0
0 to 10
10 to 20
20 to 30
>30
Distance of the nuclei from VS (μm)

Figure S3

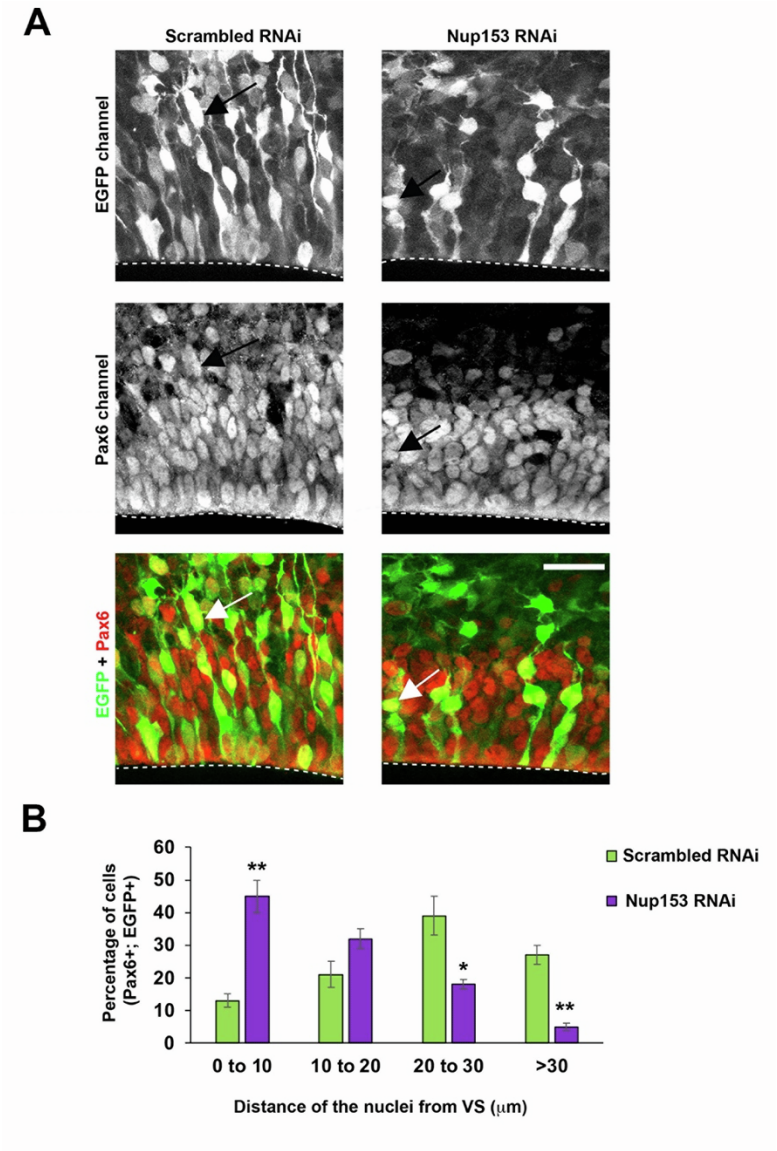
A
Scrambled RNAi
Nup153 RNAi
EGFP channel
Pax6 channel
EGFP + Pax6
B
Percentage of cells (Pax6+; EGFP+)
60
50
40
30
20
10
0
**
*
**
0 to 10
10 to 20
20 to 30
>30
Distance of the nuclei from VS (μm)
Scrambled RNAi
Nup153 RNAi

Figure S4

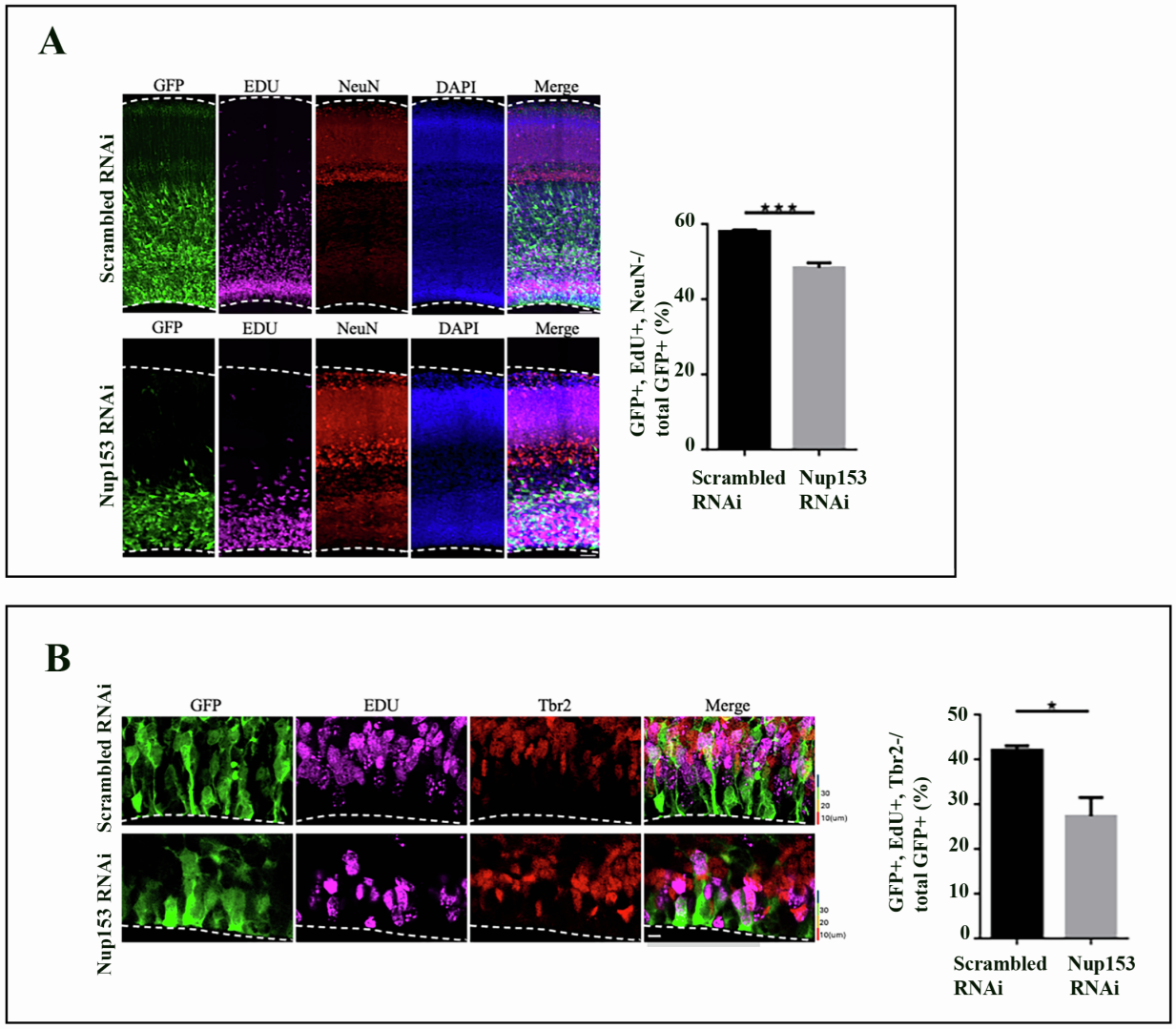
A
GFP
EDU
NeuN
DAPI
Merge
Scrambled RNAi
Nup153 RNAi
***
GFP+, EdU+, NeuN-/ total GFP+ (%)
60
40
20
0
Scrambled RNAi
Nup153 RNAi
B
GFP
EDU
Tbr2
Merge
Scrambled RNAi
Nup153 RNAi
30
20
10(um)
*
GFP+, EdU+, Tbr2-/ total GFP+ (%)
50
40
30
20
10
0
Scrambled RNAi
Nup153 RNAi

Figure S5

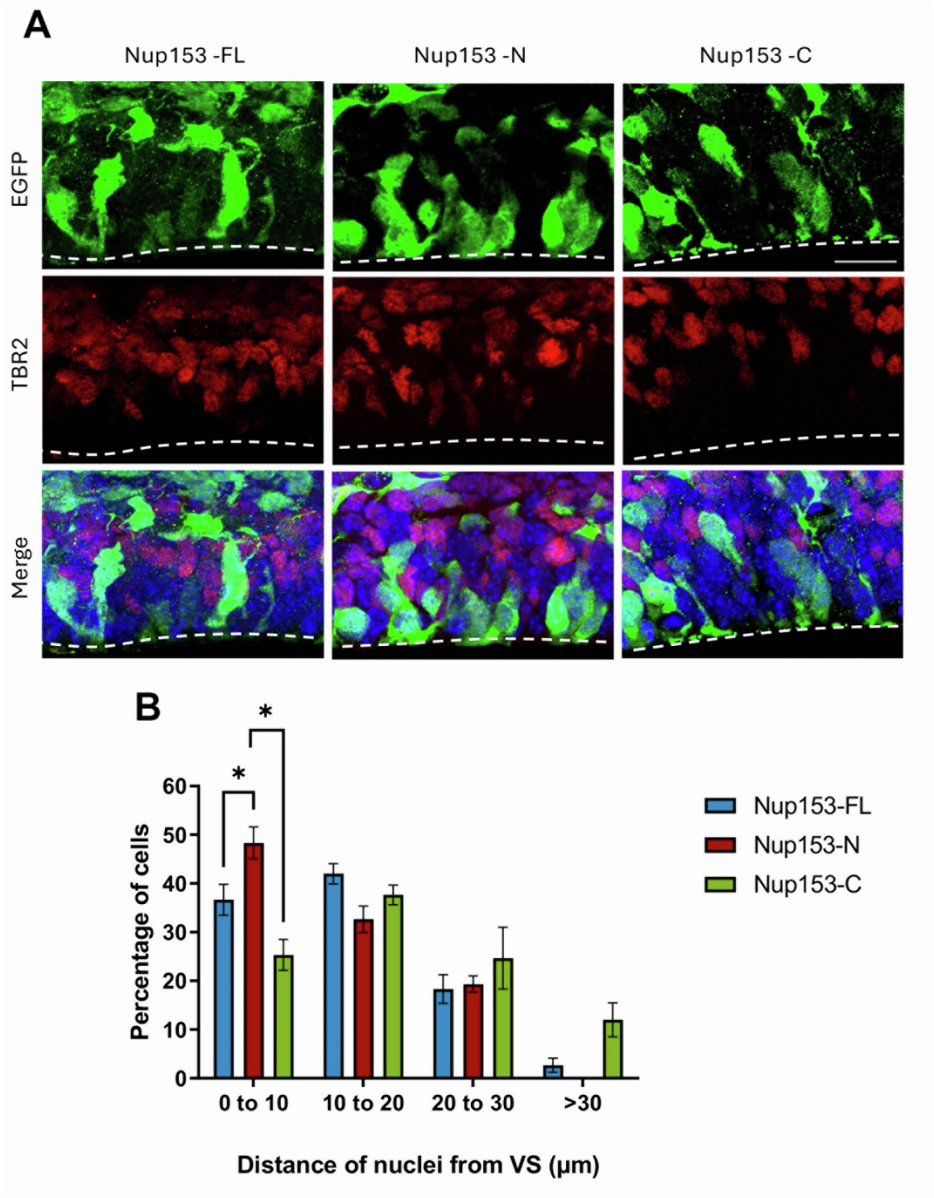
A
Nup153 -FL
Nup153 -N
Nup153 -C
EGFP
TBR2
Merge
B
Percentage of cells
60
50
40
30
20
10
0
*
*
0 to 10
10 to 20
20 to 30
>30
Distance of nuclei from VS (μm)
Nup153-FL
Nup153-N
Nup153-C

Figure S6

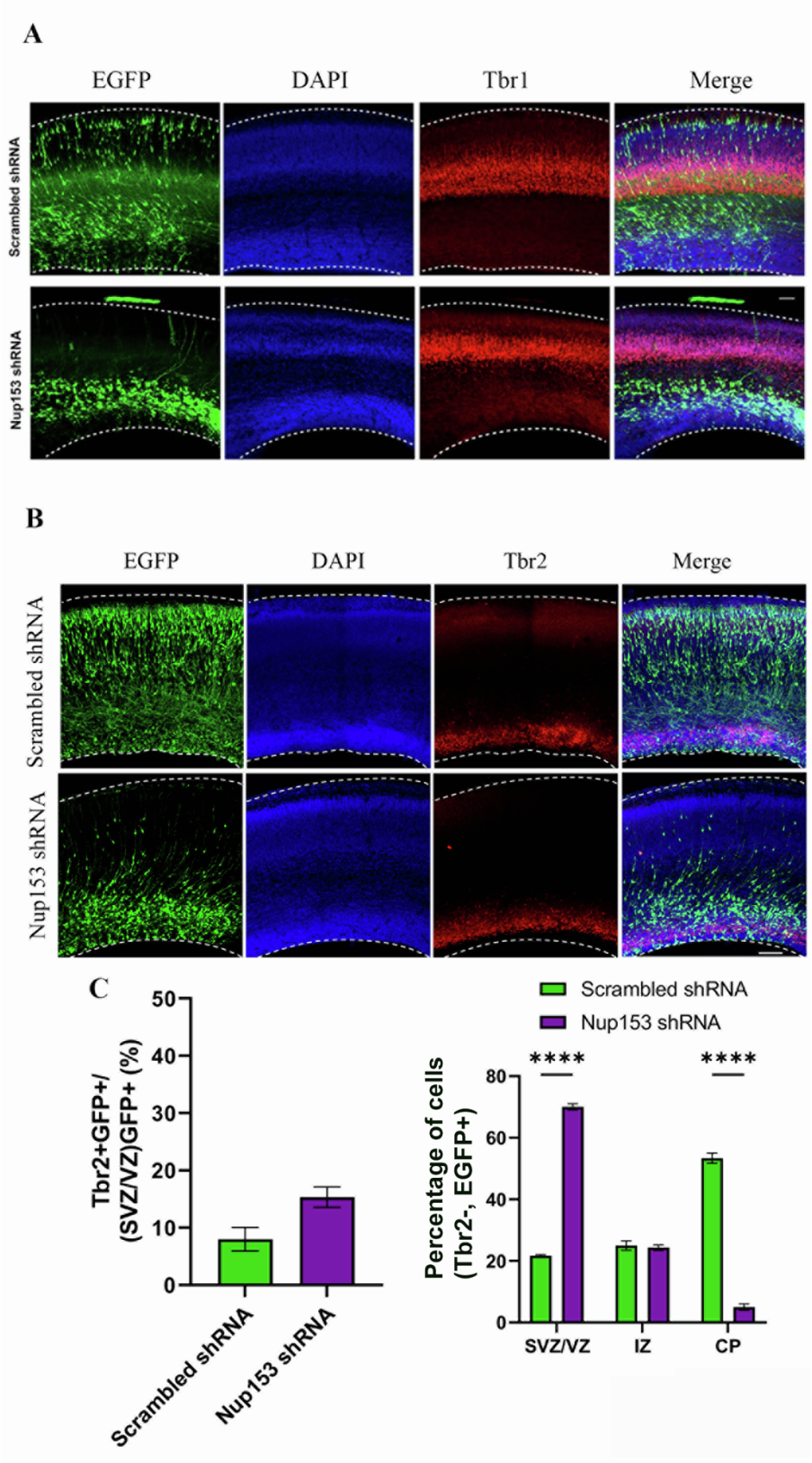
A
EGFP
DAPI
Tbr1
Merge
Scrambled shRNA
Nup153 shRNA
B
EGFP
DAPI
Tbr2
Merge
Scrambled shRNA
Nup153 shRNA
C
Tbr2+GFP+/ (SVZ/VZ)GFP+ (%)
50
40
30
20
10
0
Scrambled shRNA
Nup153 shRNA
Scrambled shRNA
Nup153 shRNA
****
****
Percentage of cells (Tbr2-, EGFP+)
80
60
40
20
0
SVZ/VZ
IZ
CP

Figure S7

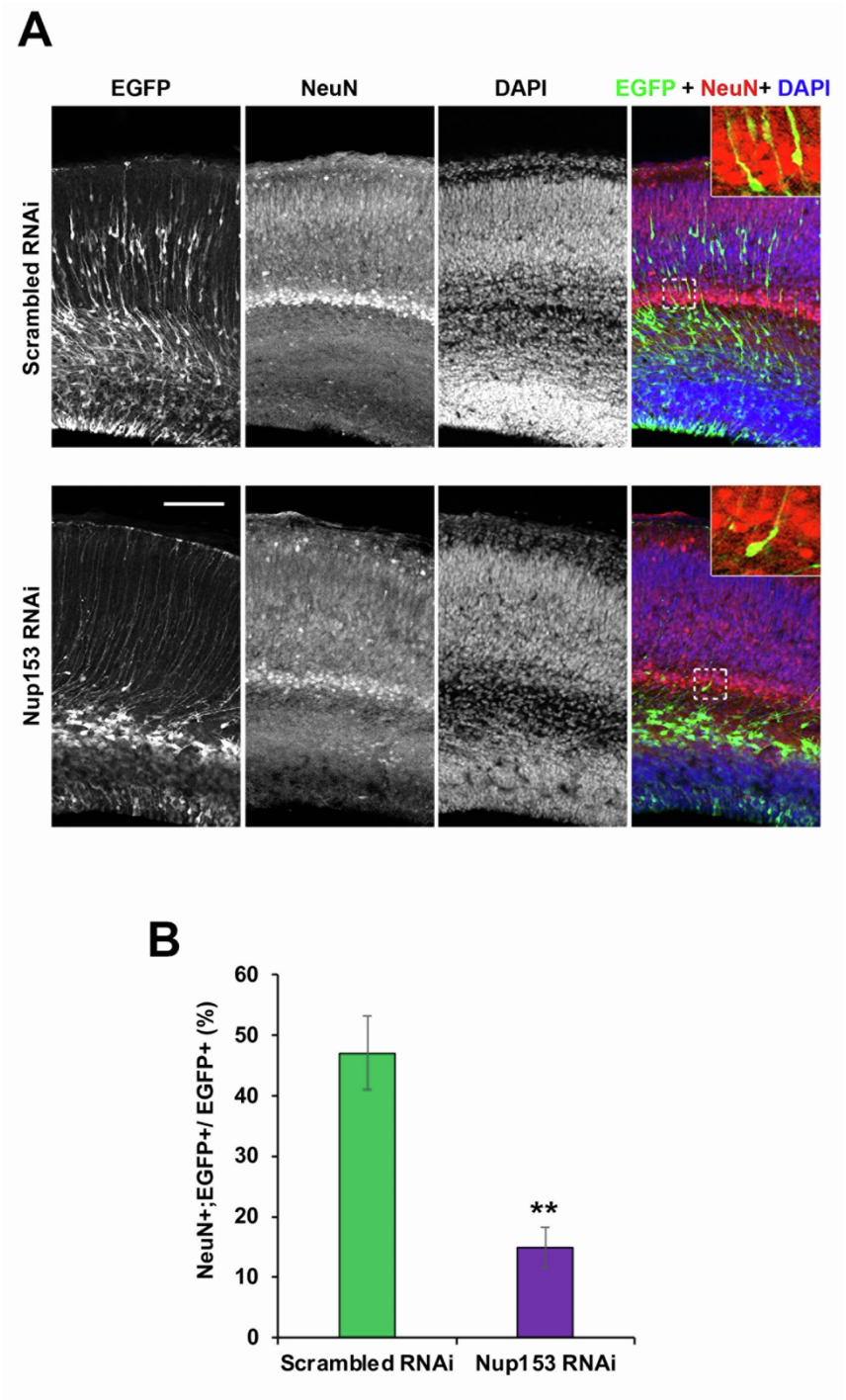
A
EGFP
NeuN
DAPI
EGFP + NeuN+ DAPI
Scrambled RNAi
Nup153 RNAi
B
NeuN+;EGFP+/ EGFP+ (%)
60
50
40
30
20
10
0
**
Scrambled RNAi
Nup153 RNAi

Figure S8

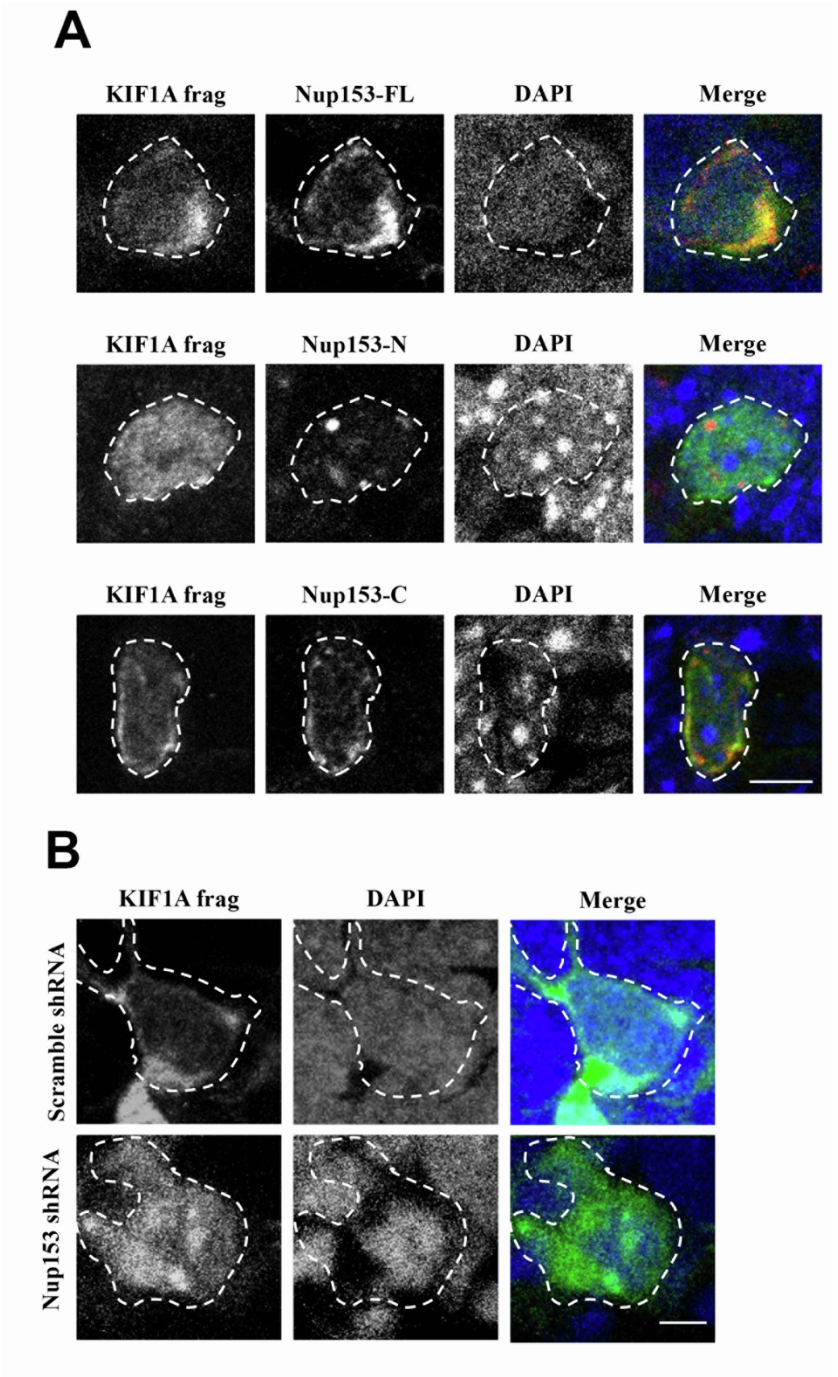
A
KIF1A frag
Nup153-FL
DAPI
Merge
KIF1A frag
Nup153-N
DAPI
Merge
KIF1A frag
Nup153-C
DAPI
Merge
B
KIF1A frag
DAPI
Merge
Scramble shRNA
Nup153 shRNA